Journal Pre-proofs

Structural studies of triazole inhibitors with promising inhibitor effects against antibiotic resistance metallo-β-lactamases

Zeeshan Muhammad, Susann Skagseth, Marc Boomgaren, Sundus Akhter, Christopher Fröhlich, Aya Ismael, Tony Christopeit, Annette Bayer, Hanna-Kirsti S. Leiros

Please cite this article as: Muhammad, Z., Skagseth, S., Boomgaren, M., Akhter, S., Fröhlich, C., Ismael, A., Christopeit, T., Bayer, A., Leiros, H.S., Structural studies of triazole inhibitors with promising inhibitor effects against antibiotic resistance metallo-β-lactamases, *Bioorganic & Medicinal Chemistry* (2020), doi: https://doi.org/10.1016/j.bmc.2020.115598

This is a PDF file of an article that has undergone enhancements after acceptance, such as the addition of a cover page and metadata, and formatting for readability, but it is not yet the definitive version of record. This version will undergo additional copyediting, typesetting and review before it is published in its final form, but we are providing this version to give early visibility of the article. Please note that, during the production process, errors may be discovered which could affect the content, and all legal disclaimers that apply to the journal pertain.

Structural studies of triazole inhibitors with promising inhibitor effects against antibiotic resistance metallo-β-lactamases

Zeeshan Muhammad[1], Susann Skagseth[2], Marc Boomgaren[1], Sundus Akhter[1], Christopher Fröhlich[2], Aya Ismael[1], Tony Christopeit[2], Annette Bayer[1,*], Hanna-Kirsti S. Leiros[2,*]

[1] Department of Chemistry, Faculty of Science and Technology, UiT The Arctic University of Norway, N-9037 Tromsø, Norway.

[2] The Norwegian Structural Biology Centre (NorStruct), Department of Chemistry, Faculty of Science and Technology, UiT The Arctic University of Norway, N-9037 Tromsø, Norway.

Corresponding authors: Annette Bayer, E-mail: annette.bayer@uit.no , Phone +47 77 64 40 69; Hanna-Kirsti S. Leiros, E-mail: hanna-kirsti.leiros@uit.no , Phone +47 77 64 57 06.

Keywords: Metallo-β-lactamase inhibitor, *N*H-triazole, inhibition properties, crystal structure, structural guided design.

Abbreviations: DMSO, dimethyl sufoxide; GIM, German imipenemase; IC$_{50}$, half maximal inhibitory concentration; IPM, imipenem; MBL, metallo-β-lactamase; NCF, nitrocefin; NDM, New Delhi metallo-β-lactamase; VIM-2, Verona integron-encoded metallo-β-lactamase.

Running Title: Triazole inhibitors hitting MBLs

20 **Abstract**

21 Metallo-β-lactamases (MBLs) are an emerging cause of bacterial antibiotic resistance by hydrolysing

22 all classes of β-lactams except monobactams, and the MBLs are not inhibited by clinically available

23 serine-β-lactamase inhibitors. Two of the most commonly encountered MBLs in clinical isolates

24 worldwide - the New Delhi metallo-β-lactamase (NDM-1) and the Verona integron-encoded metallo-

25 β-lactamase (VIM-2) - are included in this study.

26 A series of several *N*H-1,2,3-triazoles was prepared by a three-step protocol utilizing Banert cascade

27 reaction as the key step. The inhibitor properties were evaluated in biochemical assays against the

28 MBLs VIM-2, NDM-1 and GIM-1, and the former show IC_{50} values down to nanomolar range were

29 confirmed. High-resolution crystal structures of four inhibitors in complex with VIM-2 revealed

30 hydrogen bonds from the triazole inhibitors to Arg228 and to the backbone of Ala231 or Asn233, along

31 with hydrophobic interactions to Trp87, Phe61 and Tyr67. The inhibitors show reduced MIC in synergy

32 assays with *Pseudomonas aeruginosa* and *Escherichia coli* strains harbouring VIM enzymes. The

33 obtained results will be useful for further structural guided design of MBL inhibitors.

34

1   Introduction

The emergence and spread of antibiotic resistant bacteria are defined as a global health problem by the World Health Organization (WHO).[1] The increase in Gram-negative antibiotic resistance bacteria is particularly worrisome. Pan-resistance or extreme drug resistance are now commonly used terms to describe clinically important isolates of *Pseudomonas aeruginosa*, *Acinetobacter baumannii* and Enterobacteriaceae that are resistant to virtually all antibiotics[2].

There are several causes for antibiotic resistance but the most common mechanism for β-lactam resistance is the presence of β-lactamases enzymes that cleave the β-lactam ring rendering the drug inactive.[3-5] Drug treatment using β-lactamase inhibitors (BLI) as adjuvants to re-potentiate antibiotics is already in clinical use, e.g. the new serine-BLI avibactam has been approved in USA as a combination treatment with ceftazidime against complicated urinary tract infections and intra-abdominal infections.[5] Other examples in the clinic are the β-lactam-BLI combinations amoxicillin-clavulanate, ticarcillin-clavulanate, ampicillin-sulbactam, and piperacillin-tazobactam.[5, 6] These BLIs inactivate primarily class A serine β-lactamase (SBL) enzymes, and avibactam also inhibits class C and some class D SBL enzymes.[5, 6]

For class B metallo-β-lactamases (MBLs) no clinically approved BLIs are available. Lately, interesting results have been reported for the thiazole-4-carboxylic acid analogue ANT431 showing promising results against NDM-1 (K_i = 0.29 μM) and VIM-2 (K_i = 0.19 μM) including *in vivo* inhibitor efficacy.[7] Other recently described inhibitors include the natural product aspergillomarasmine,[8] which showed *in vivo* inhibitor efficacy against NDM-1, azolylthioacetamides[9] with K_i (NDM-1) = 0.43 μM, bisthiazolidines[10] with K_i (NDM-1) = 7-19 μM and 1,2,4-triazole-3-thiones with K_i (NDM-1) = 0.72 μM.[11, 12] However, the clinical need for an MBL inhibitor is still outstanding.

Fokin and coworkers reported that 1,2,3-*N*H-triazoles of the general formula **1** were promising VIM-2 inhibitors.[13, 14] In their study, the best compounds (**1cc`** and **1cd`**) showed sub-micromolar activity (IC$_{50}$ = 0.07 μM; K_i = 0.02 μM) against VIM-2, and were able to re-potentiate the β-lactam antibiotic imipenem in VIM-2 producing *Escherichia coli* (BL21) cells when tested at 150 μM concentration.[13] Based on docking studies, they predicted **1** to bind to the VIM-2 active site through the sulfonyl group as a zinc binding group. We became interested to gain insight into the inhibitory action of the 1,2,3-*N*H-triazoles **1** in order to further explore the potential of this scaffold as MBL inhibitors. With our experience in crystallization of inhibitors with MBLs[15-17] we aimed for crystallographic studies of enzyme–inhibitor complexes to understand the mode of binding and low IC$_{50}$ values exhibited by the

66 1,2,3-*N*H-triazoles **1**. The exact interactions involved in the substrate binding of VIM- 2 are not clear,

67 since no crystal structure in complex with a substrate has been reported.

68
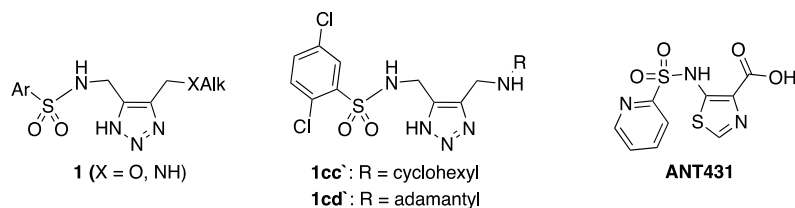
69 Here, we report the synthesis of a small focussed library of new and reported[13, 14] (**1cc'**, **1cd'**, **1dg'**,

70 **1dh'**) analogues of 1,2,3-*N*H-triazoles and our investigation of their potential as inhibitors of the

71 previously reported VIM-2, and additionally NDM-1, a clinically important MBL, and GIM-1. The

72 compounds were evaluated in biochemical and cell-based assays, and for the most promising

73 compounds the inhibitory effect in synergy with meropenem was tested against clinical strains of *P.*

74 *aeruginosa* (VIM-2)*, K. pneumoniae* (NDM-1) and *E. coli* (VIM-29). We obtained crystal structures of

75 four inhibitors in complex with VIM-2. In addition, a structure activity relationship (SAR) analysis of the

76 observed inhibition patterns is provided using reported crystal structures of the three target enzymes

77 (NDM-1 complex with hydrolysed ampicillin [18], VIM-2 in complex with fragments [17] and wild type GIM-1

78 [19]).

2   Results and discussion

2.1 Synthesis of NH-1,2,3-triazole inhibitors

81 A small library of *N*H-1,2,3-triazoles **1aa'–1dj'** were synthesized as shown in Scheme 1A.[13] Treatment

82 of 4-chlorobutyneamine **2** with sulfonyl chlorides and base (K_2CO_3) provided the chlorosulfonamides

83 **3a-d**, which were converted to the respective azidosulfonamides **4a-d**. The crude azides **4a–d**

84 containing different sulphonamide groups (R^1 in red) underwent the Banert cascade[20-22] to *N*H-triazole

85 sulphonamides **1aa'-di'** in the presence of a range of nucleophiles (R^2 in blue). For a mechanistic

86 proposal of the Banert cascade see Scheme 1B.[21, 23, 24] The acetate substituted triazole **1dj'** was

87 prepared by acetylation of the corresponding alcohol obtained from cyclisation with water as

88 nucleophile.

89

A: Synthetic pathway[13]

B: Mechanistic view of the Banert cascade[21, 23, 24]

90
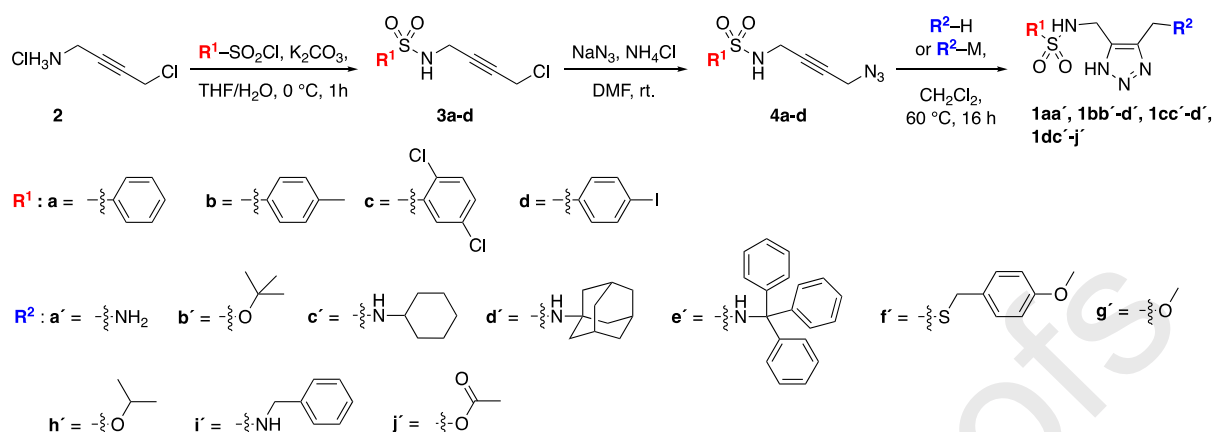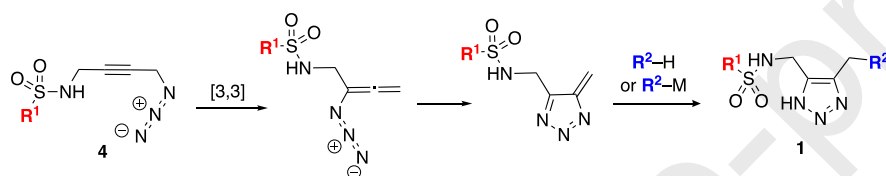
91 **Scheme 1**. Synthesis and structures of *N*H-1,2,3-triazole based inhibitors.

92 *2.2 Characterization of inhibitor properties against VIM-2, GIM-1 and NDM-1*

93 The inhibitory activities of the *N*H-1,2,3-triazoles **1aa'–1dj'** against the MBLs NDM-1, VIM-2 and GIM-

94 1 were evaluated as the half maximal inhibitory concentration (IC$_{50}$) values in biochemical competition

95 assays (**Table 1**). For VIM-2 and GIM-1, the IC$_{50}$ values were measured using nitrocefin as a reporter

96 substrate, while IC$_{50}$ values for NDM-1 were measured with imipenem as reporter substrate. Nitrocefin

97 is hydrolysed by NDM-1 with a too high catalytic efficiency and is unsuitable as a reporter substrate

98 for NDM-1.[25] The sequence identity between the three MBL enzymes used is 28% for VIM-2 versus

99 GIM-1, 32% between VIM-2 and NDM-1 and 24% between NDM-1 and GIM-1.[15]

100 Compounds **1cc'**, **1cd'**, **1dg'** and **1dh'** have been evaluated as VIM-2 inhibitors by Fokin and coworkers

101 resulting in IC$_{50}$ values of 0.07 μM for **1cc'**, **1cd'** and **1dh'** and 7.3 μM for **1dg'**,[13] which were similar to

102 our IC$_{50}$ values of 0.23 (**1cc'**), 0.12 (**1cd'**), 0.53 (**1dh'**) and 15 (**1dg'**) μM (**Table 1**). When these triazoles

103 were investigated against GIM-1, the inhibition was poor for **1dg'** (IC$_{50}$ = 169 μM) and **1dh'** (IC$_{50}$ = 193

104 μM) and no inhibition was observed for **1cc'** and **1cd'** and none of the four triazoles (**1cc'**, **1cd'**, **1dg'**

105 and **1dh'**) were active against NDM-1.

106 Investigation of an extended library containing triazoles **1aa'-dj'** confirmed the observation that the

107 compounds with the general structure of **1** were selective VIM-2 inhibitors with IC$_{50}$s from 0.07–23

108   µM, while inhibition of GIM-1 and NDM-1 was generally weaker. GIM-1 was inhibited by 9 compounds

109   (IC_{50}s from 18–353 µM) with **1dd'** (IC_{50} = 18 µM) being the best inhibitor. The reason for the weak

110   inhibition of GIM-1 is not obvious and other inhibitor classes showed good inhibition towards GIM-1

111   in this assay.[15] Only 7 compounds were active against NDM-1 (IC_{50}s from 81–231 µM) with **1de'** (IC_{50} =

112   81 µM) being the most active compound.

113   The most potent VIM-2 inhibitors **1cc'** and **1cd'** (R^1 = 2,5-dichlorophenyl and **1dc'** and **1dd'** (R^1 = 4-

114   iodophenyl) showed high nanomolar inhibition (IC_{50} = 0.067–0.23 µM). These compounds are

115   structurally similar as they contain halogenated aromatic R^1 substituents although with different

116   spatial arrangement (2,5-substitution compared to 4-substitution) and cyclic alkyl amino groups as R^2

117   substituents (cyclohexyl or adamantly), which may explain the similar inhibition properties.

118   The library contained two series of compounds containing identical R^2 groups; one consisting of **1bc'**

119   (IC_{50} = 1.5 µM), **1cc'** (IC_{50} = 0.23 µM) and **1dc'** (IC_{50} = 0.067 µM) with R^2 like cyclohexylamino and the

120   other consisting of **1bd'** (IC_{50} = 2.3 µM), **1cd'** (IC_{50} = 0.12 µM), and **1dd'** (IC_{50} = 0.16 µM) with R^2 like

121   adamantylamino. Comparison of the compounds in a series provided an indication that the

122   halogenated R^1 groups of compounds **1cc'/1cd'** (R^1 = 2,5-dichlorophenyl) and **1dc'/1dd'** (R^1 = 4-

123   iodophenyl) were slightly advantageous (a 5–10-fold reduction in IC_{50}s) over the hydrocarbon based R^1

124   group of compounds **1bc'/1bd'** (R^1 = 4-methylphenyl).

125   A wide range of R^2 substituents were investigated in the **1d** series (**Table 1**). The inhibition of VIM-2

126   varied from IC_{50} of 0.07 µM for **1dc'** (R^2 = cyclohexylamino) to IC_{50} > 250 µM for **1de'** with the very

127   bulky triphenylmethylamino group as R^2 substituent. In the middle range (IC_{50} = 15–21 µM), we found

128   inhibitors **1df'** (R^2 = 4-methoxybenzylsulfide), **1dg'** (R^2 = *iso*-propoxy) and **1dj'** (R^2 = acetate) with

129   structurally very different R^2 substituents. Unfortunately, inhibitor **1di'** with benzylamine as R^2

130   substituent resulted in precipitation.

131   *2.3 Evaluation of inhibitors in bacterial cell assays, with whole E. coli cells and synergy assays*

132   To investigate the inhibitory activity against MBLs in bacterial cells, two different assays were used.

133   The first was *E. coli* SNO3 cells transformed with bla_{VIM-2}, bla_{GIM-1} or bla_{NDM-1} (**Table 1**). The enzyme

134   production was induced by addition of IPTG. The inhibitory activity was measured as the difference in

135   speed of hydrolysis of the reporter substrate between the presence and absence of inhibitor, according

136   to equation 1. A high degree of inhibition then indicate that the inhibitor prevents the MBL hydrolytic

137   activity of breaking down the reporter substrate, but works as an inhibitor in a cell.

138   The inhibitory activities against VIM-2 in bacterial cells of **1aa'-1dj'** (**Table 1**) varied from 95% inhibition

139   to inactive and were in good agreement with the inhibition determined in the biochemical assay. The

140   most active inhibitors (**1bb'**, **1bc'**, **1cc'**, **1cd'**, **1dc'** and **1dd'**) determined in the biochemical assay (IC$_{50}$

141   from 0.07–2.3 µM) gave 82–96% inhibition in the cell based assay, except for **1cd'**, where no inhibition

142   was found in the whole cell assay. This indicates that the inhibitors cross the outer *E. coli* membrane

143   and hit VIM-2 localized in the periplasmic space. The reason for **1cd'** only being active towards purified

144   VIM-2 (IC$_{50}$=0.12 µM) and not in the whole cell assay (with VIM-2), can be that this inhibitor did not

145   cross the outer *E. coli* membrane which is different from the most active inhibitors.

146   For GIM-1 producing *E. coli* SNO3 cells**,** we observed much lower levels of percent inhibition for

147   inhibitors **1aa'**-**1dj'** with 3-25% in agreement with the higher IC$_{50}$ values observed against this enzyme

148   compared to VIM-2 (**Table 1**). The highest percent inhibition was obtained for **1df'** with 33%. In the

149   NDM-1 whole cell assay, the percent inhibition was further decreased with most of the investigated

150   compounds showing no inhibition (**Table 1**). Only inhibitors **1dd'** and **1df'** showed inhibitor properties

151   with 17% and 34% inhibition, respectively.

152   Additionally a second cell based assay was performed where the inhibitory effect in synergy with

153   meropenem of **1cc'**, **1dc'** and **1dj'** was tested against clinical strains of *P. aeruginosa* (VIM-2)*, K.*

154   *pneumoniae* (NDM-1) and *E. coli* (VIM-29) (**Table 2**)*.* Not surprising, none of the tested inhibitors

155   affected the NDM-1 producing *K. pneumoniae* strain. Inhibitor **1cc'** gave a reduced MIC from 64 to 8

156   mg/L in VIM-2 producing *P. aeruginosa*, but did not affect the *E. coli* strain. Our most promising hit is

157   **1dj'**, which at low inhibitor concentration (50 mM) lowered the MIC from 64 to 1 mg/L for VIM-2

158   producing *P. aeruginosa* and from 16 to 1 mg/L for VIM-29 producing *E. coli*. VIM-2 and VIM-29 have

159   90% sequence identity, thus it is likely that an *E. coli* producing VIM-29 could also be inhibited and give

160   a reduce MIC. In the synergy assay meropenem was the reporter substrate. The own effect from the

161   inhibitors (>500 µM) did not show any toxicity (data not shown).

162   *2.4 Triazole inhibitors bound to VIM-2 in crystal structure complexes*

163   Crystal structures of VIM-2 in complex with the inhibitors **1cc'**, **1dh'**, **1di'** and **1dj'** were used to

164   investigate the interactions involved in the binding of the inhibitors. For the inhibitors **1cc'**, **1dh'** and

165   **1di',** the DMSO-free co-crystallization method [16] was applied to obtain complex structures, whereas

166   the inhibitor **1dj'** was soaked into native VIM-2 crystals.

167   The complex structures with the inhibitors **1cc'** and **1dh'** crystallized in the space group P2$_1$2$_1$2 with

168   one protein molecule in the asymmetric unit. The two other complexes structures crystallized in the

169   space group C2 with two protein molecules in the asymmetric unit. Space group C2 has previously

170   been reported for VIM-2 [17], but space group P2$_1$2$_1$2 has not been observed before. The resolution of

171   the obtained structures was ≤ 1.5 Å, with the complex structure VIM-2_**1cc'** showing the best

172 resolution of 1.07 Å. To our knowledge, this is the highest resolution structure so far reported for VIM-

173 2. Details on the statistics for the data collection and the refinement are shown in **Table 3** and **Table**

174 **4**.

175 Overall the protein structures as well as active site conformations of the obtained VIM-2 complexes

176 were all in accordance with previously reported structures and no major differences were noticed. [15-

177 17, 26-28] The crystal structures with the inhibitors **1dh'** and **1cc'** showed unassigned electron density in

178 the active site of the enzyme, clearly corresponding to the inhibitors (**Figure 2A** and **D**). Also, the

179 structures with inhibitors **1di'** and **1dj'** showed unassigned electron density in the active site of one or

180 both VIM-2 protein molecules, respectively. However, this electron density was less well defined and

181 more ambitious to interpret, reflecting a lower occupancy and a higher degree of disorder of the bound

182 inhibitors (**Figure 2G** and **K**). Several of the structures showed radiation damages,[29-31] caused to

183 interactions between the bright synchrotron X-ray beam and the protein in the crystal. This is seen as

184 positive peaks in the difference Fourier electron density maps. Upon radiation damage, the absorbed

185 energy is dissipated as covalent bond breakage and heat resulting in higher thermal vibration. In the

186 complex structure with the inhibitor **1dh'** and **1cc'**, the Cys221 was partially oxidized to the cysteine

187 sulfonate, a radiation damage previously observed for VIM-2[17, 28]. Furthermore, radiation damage in

188 the iodine-carbon bound in the inhibitors **1dh', 1di'** and **1dj'** was observed, most likely due to electron

189 capture. [30]

190 The position of the four inhibitors in the active site of VIM-2 and the interactions with the protein are

191 shown in **Figure 2**. A common feature in the binding mode of all inhibitors was the orientation of the

192 *N*H-1,2,3-triazole moiety and the sulfonamide group. The triazole moiety directly interacted with one

193 of the two zinc ions in the active site and with the bridging hydroxide ion. In addition, one of the

194 nitrogen atoms in the triazole ring formed an interaction with Arg228 through a hydrogen bond. The

195 sulfonamide group occupied slightly different positions in the complex structures of **1cc'**, **1dh'**, **1di'** and

196 **1dj'** (conformation A). However, the main orientation was similar and allowed hydrogen bond

197 interactions with the protein backbone of Ala231 and/or Asn233. Previously reported docking studies

198 with arylsulfonamid-NH-123-triazoles suggested that either the sulfonamide group[13, 14] or the triazole

199 ring[32] interact with the zinc ions in the active site. Furthermore, in all docking studies the hydroxide

200 ion bridging the two zinc ions was replaced by the inhibitor. In contrast, our results clearly show that

201 the hydroxide ion is not replaced by the inhibitors and that the triazole moiety interacts only with one

202 of the two zinc ions (Zn2), whereas the sulfonamide group does not participate in the zinc binding.

203 The inhibitors **1dh'**, **1di'** and **1dj'** have a 4-iodophenyl group in the R^2 position towards His263 and

204 Arg228. In all complex structures with these inhibitors, the iodine-carbon bond was radiation damaged

205 and the electron density map clearly showed that the iodine was separated from the inhibitor (**Figure**

206 **2D, G** and **K**). These radiation damages most likely induced changes in the orientation of the benzene

207 ring as well as the iodine, as also observed for a brominated DNA/RNA hybrid.[30] Hence, the

208 interpretation of the interactions with the iodophenyl group was difficult. However, the results

209 indicate that the moiety forms hydrophobic interaction with Tyr67 and His263. Furthermore, the

210 benzene ring might form a cation-π stacking with Arg228. In the inhibitor **1cc'**, the iodobenzene moiety

211 in position R^2 is replaced by a dichlorobenzene, which adopts two different conformation. In both

212 conformations, the benzene ring forms hydrophobic interactions with the Tyr67, with conformation A

213 adopting an orientation better suited for a π-π stacking. In addition, one of the chlorine ions interacts

214 in both conformations with Arg228 and in conformation B with the backbone of Ala231.

215 All four inhibitors have different substituents in the R^1 position towards Trp87. The inhibitor **1cc'** has a

216 cyclohexylamine moiety at this position. The cyclohexyl ring of the moiety interacts with His118, Trp87

217 and Phe61, and the amine nitrogen interacts with the hydroxide ion located between the two active

218 site Zn ions (**Figure 2B, C**) through a hydrogen bond. Similar interactions were observed both for

219 inhibitor **1dh'** between the catalytic hydroxide ion and the oxygen of the isopropoxy moiety (**Figure**

220 **2E, F**) and for inhibitor **1di'** involving the nitrogen of the benzylamino group (**Figure 2H, I**). In the latter

221 complex structure, the benzene ring of the benzylamino group additionally seems to interact with

222 Trp87, Phe61 and Tyr67. However, for the benzylamino group of **1di'** and the methyl acetate moiety

223 of **1dj'**, only weak electron densities were observed. Hence, the interpretation of the exact orientations

224 and the interactions with the protein were difficult. The low electron density and the disordered

225 structure might indicate that these moieties do not form strong interactions with the protein.

226 The binding interactions identified in the above VIM-2 inhibitor complexes may explain the reduced

227 inhibitor activity of the NH-triazoles towards NDM-1 and GIM-1. The important reside determinants in

228 the NDM-1 binding site are Phe63, Lys224 and Ala228 (see e.g. [15]). In the VIM-2 inhibitor complexes

229 we observed hydrophobic interactions with Tyr67 and cation-π stacking interactions with Arg228,

230 which both are not possible with the corresponding Val67 and Lys224, respectively, in NDM-1. On the

231 other hand, the hydrogen bonding interaction of the NH-triazole to Arg228 in VIM-2 may be possible

232 with the adjacent Lys224 in NDM-1. The GIM-1 the binding site includes Tyr64, Val76, Arg224 and

233 Trp228. For GIM-1, the guanidino group of Arg224 overlaps with the corresponding group of Arg228

234 in VIM-2 making hydrogen bonding to the NH-triazole possible. However, Tyr64 in GIM-1 is too far

235 away to replace the nice π-π stacking involving Tyr67 in VIM-2, thus might explain the lower inhibitor

236   potential with high IC$_{50}$ values for GIM-1. Moreover, VIM-29 (UniProt J7HGI2), present in the *E. coli*

237   strain used for the synergy assay, carries Tyr67, His224 and Ser228, so the polar His228 and aromatic

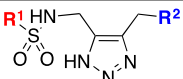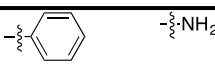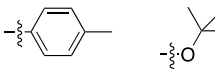238   Tyr67 could allow for good inhibitor binding and support the low MIC in the synergy assays (Table 2).
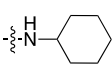
239   **3   Conclusion**
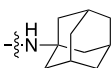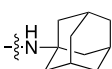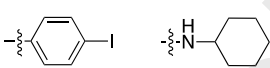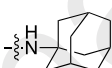
240   Inspired by encouraging results on using triazoles as MBL inhibitors, we prepared a small focused

241   chemical library with 15 *N*H-1,2,3-triazole molecules, which was tested for inhibitory against VIM-2,

242   GIM-1 and NDM-1.

243   We found that VIM-2 was inhibited by several NH-1,2,3-triazole and the new inhibitor **1dc'** gave nano-

244   molar affinity with IC$_{50}$ of 0.067 µM. This inhibitor also affected GIM-1 (IC$_{50}$=69 µM) and NDM-1

245   (IC$_{50}$=148 µM), but to a much lower extent.

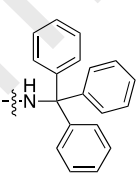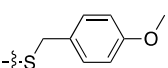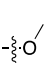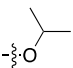246   The most promising inhibitor was **1dj'** with moderate IC$_{50}$ values of 23 µM (VIM-2), 48 µM (GIM-1) and

247   231 µM (NDM-1). More interestingly, the synergy assay found **1dj'** to effects two clinical isolates. One

248   *P. aeruginosa* producing VIM-2 reduced the MIC from 64 mg/L with only meropenem to only 1 mg/L

249   for meropenem and **1dj'**; and an *E. coli* producing VIM-29 showed reduced MIC from 16 mg/L (only

250   meropenem) to 1 mg/L when combining meropenem and **1dj'**. The 1.50 Å complex structure of VIM-

251   2_**1dj'** show tight aromatic π-π stacking to Tyr67, binding from the NH-1,2,3-triazole group to Arg228

252   and the active site Zn2 ion, and the presence of the hydroxyl ion between the two zinc ions. Our new

253   complex structure of VIM-2_**1dj'** is therefore a valuable starting point for structure guided inhibitor

254   design of a new inhibitor targeting several MBL enzymes simultaneously.

255

256 **Tables and figures:**

257 *Table 1. The molecular structures of the synthesized inhibitors with measured inhibition concentrations*
258 *(IC_{50}) against pure VIM-2, GIM-1 and NDM-1 enzymes; followed by %inhibition (equation 1) in* E. coli
259 *SNO3 bacterial whole cell experiments with bla_{VIM-2}, bla_{GIM-1} or bla_{NDM-1}.*

R[1]	R[2]	VIM-2 [a]		GIM-1 [a]		NDM-1 [b]	
		IC_{50} (μM) [a]	% inhib [a]	IC_{50} (μM) [a]	% inhib [a]	IC_{50} (μM)	% inhib
1aa'	-NH2	23	29	NI	NI	NI	NI
1bb'	-O	7.2	60	128	4.5	142	NI
1bc'	-N-cyclohexyl	1.5	82	NI	2.3	144	NI
1bd'	-N-adamantyl	2.3	84	83 (67)	NI	ND	NI
1cc'*	-N-cyclohexyl	0.23	94	NI	7	98	NI
1cd'	-N-adamantyl	0.12	NI	P (7.7)	21	ND	NI
1dc'	-N-cyclohexyl	0.067	95	69	3	148	NI
1dd´	-N-adamantyl	0.16	96	18	22	ND	17
1de'	-N-trityl	>250	19	353	3	81	NI
1df'	-S-benzyl-OMe	21	45	227	33	ND	34
1dg'	-O	15	51	169	11	NI	NI
1dh'*	-O-iPr	0.53	85	193	11	NI	NI

- 11 -

1di'*		P	ND	ND	ND	ND	ND
1dj'*		23	ND	48	ND	231	ND

260 [a] the reported substrate was nitrocefin; [b] the reported substrate was imipenem; NI: no observable
261 inhibition; ND: not determined; P: precipitated. * A VIM-2 complex structure is reported here.
262

263

264 *Table 2. Synergy test of selected inhibitors against clinical strains containing VIM-2, NDM-1 or VIM-29*
265 *and meropenem (MEM) or MEM and inhibitor to determine the MIC in mg/L. The inhibitor*
266 *concentration was 50 µM (**1cc'**, **1dj'**) or 125 µM (**1dc'**).*

Ref. no	K34-7	K66-45	50639799
Species	*P. aeruginosa*	*K. pneumoniae*	*E. coli*
MBL	VIM-2	NDM-1	VIM-29
	MIC (mg/L)	MIC (mg/L)	MIC (mg/L)
MEM	64	32-64	16
MEM+1cc'*	8	32	16
MEM+1dd'	16	32	nd
MEM+1dc'	8	64	nd
MEM+1dh'*	P	P	P
MEM+1di'*	P	P	P
MEM+1dj'*	1	64	1

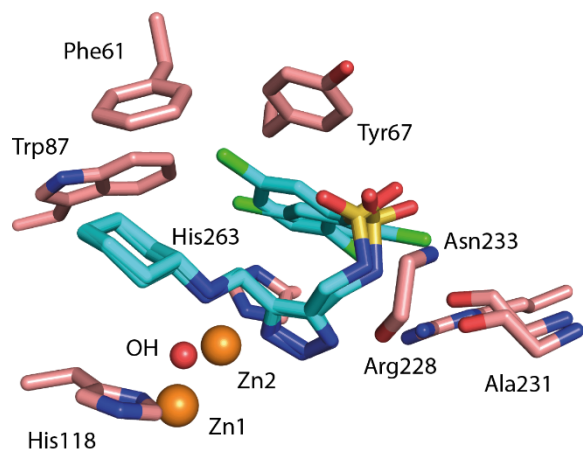267 * a VIM-2 complex structure is reported here. nd: not determined.
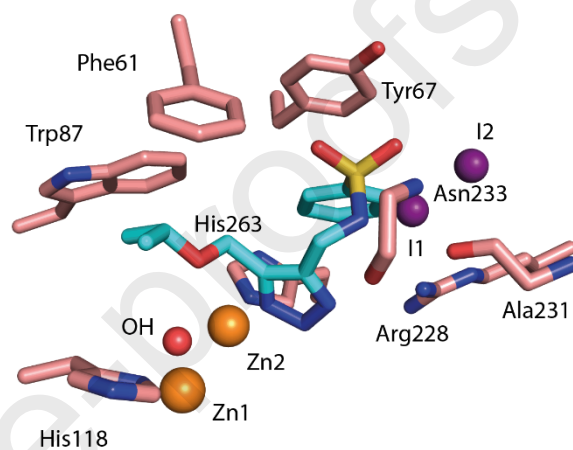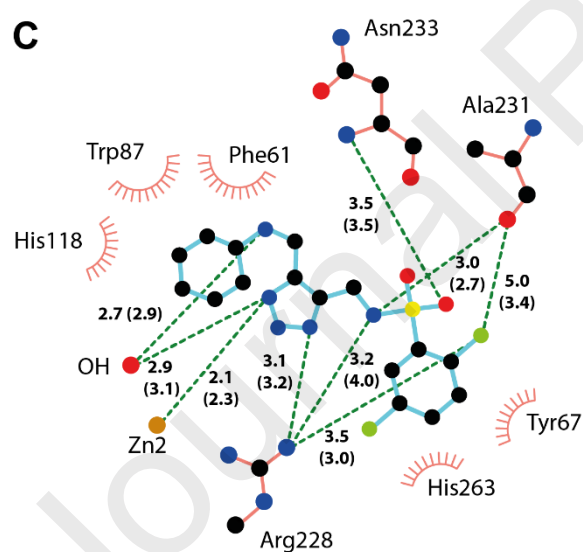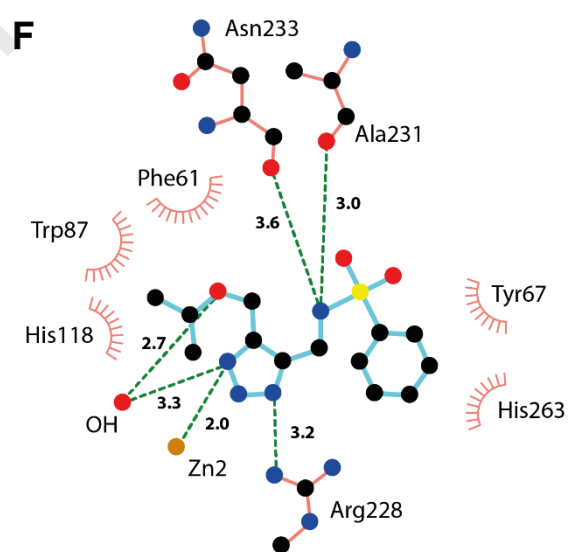
268 P: precipitated

269

270 *Table 3. X-ray data collection statistics for VIM-2 in complex with compound **1cc'**, **1dh'**, **1di'** and **1dj'**.*
271 *Values in parenthesis are for the highest resolution shell.*

	VIM-2_**1cc'**	VIM-2_**1dh'**	VIM-2_**1di'**	VIM-2_**1dj'**
Diffraction source	ID23-1, ESRF	ID23-1, ESRF	ID29, ESRF	ID29, ESRF
Wavelength (Å)	0.97625	0.97625	0.983998	0.983998
Temperature (°C)	-173	-173	-173	-173
Crystal-detector distance (mm)	158.67	201.24	275.00	275.00
Rotation range per image (°)	0.15	0.1	0.05	0.1
Total rotation range (°)	135	130	130	180
Exposure time per image (s)	0.037	0.037	0.04	0.037
Space group	$P\ 2_1 2_1 2$	$P\ 2_1 2 2_1$	C2	C2
a, b, c (Å)	98.35, 44.34, 60.84	90.75, 45.81, 63.93	100.59, 79.03, 67.24	101.28, 79.27, 67.69
γ (°)	90.00	90.00	130.09	130.35
Resolution range (Å)	38.26-1.07 (1.10-1.07)	52.26-1.40 (1.43-1.40)	31.33-1.50 (1.52-1.50)	39.63-1.50 (1.52-1.50)
No. of unique reflections	115206	52181	61683	64863
Multiplicity	4.8 (4.5)	4.7 (4.6)	2.5 (2.5)	3.4 (3.3)
Completeness (%)	97.8 (93.6)	98.3 (87.4)	95.8 (98.0)	99.5 (100)
R_{merge} (%)	6.4 (100)	6.3 (10.5)	4.8 (27.9)	7.2 (87.9)
Mean $\langle I/\sigma_{(I)} \rangle$	11.4 (1.5)	13.0 (1.5)	11.5 (2.7)	9.4 (1.2)
Overall *B*-factor from Wilson plot (Å^2)	10.41	17.31	13.60	16.38

272

273

274 *Table 4. Crystallographic refinement statistics for VIM-2 in complex with compounds* **1dd'**, **1ei'**, **1ej'** *and*
275 **1ek'**.

	VIM-2_**1cc'**	VIM-2_**1dh'**	VIM-2_**1di'**	VIM-2_**1dj'**
PDB entry	6TM9	6TMC	6TMB	6TMA
Final R_{work} (%)	11.01	13.16	13.87	15.74
Final R_{free} (%)	12.50	15.80	16.42	19.54
Molecules in asymmetric unit	1	1	2	2
No. of non-H atoms				
Protein	1989	1888	3676	3600
Ions	2 Zn^{2+}, 1 Cl$^-$, 1 OH$^-$	2 Zn^{2+}, 1 Cl$^-$, 1 OH$^-$	6 Zn^{2+}, 4 Cl$^-$, 2 OH$^-$	6 Zn^{2+}, 4 Cl$^-$, 2 OH$^-$
Ligand	52 (2 conformations)	23	26	86 (2 conformations)
Water	526	344	662	627
R.m.s. deviations				
Bonds (Å)	0.010	0.012	0.010	0.005
Angles (°)	1.217	1.005	1.016	0.748
Average B factors (Å^2)				
Protein	13.87	20.9	17.32	22.72
Ion	10.94	17.3	21.80	27.94
Ligand (occupancy)	14.56 (0.6/0.3)	22.9 (0.86)	46.61 (0.78)	64.31 (0.51/0.49)
Water	33.16	38.6	34.46	37.53
Ramachandran plot				
Most favoured (%)	97.12	96.9	97.75	97.93
Allowed (%)	2.06	2.2	2.25	1.61

A

D

B

Phe61

Trp87

Tyr67

His263

Asn233

Arg228

Ala231

OH

Zn2

Zn1

His118

E

Phe61

Trp87

Tyr67

I2

Asn233

I1

His263

Arg228

Ala231

OH

Zn2

Zn1

His118

C

Asn233

Ala231

Trp87   Phe61

His118

3.5
(3.5)

3.0
(2.7)

5.0
(3.4)

2.7 (2.9)

3.1
(3.2)

3.2
(4.0)

OH

2.9
(3.1)

2.1
(2.3)

Zn2

3.5
(3.0)

Tyr67

His263

Arg228

F

Asn233

Ala231

Phe61

Trp87

His118

3.6

3.0

Tyr67

2.7

His263

OH

3.3

2.0

3.2

Zn2

Arg228

277

278
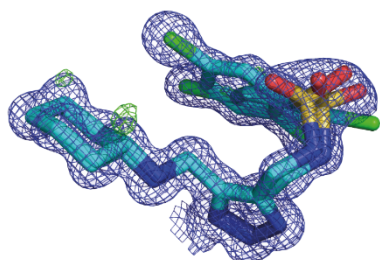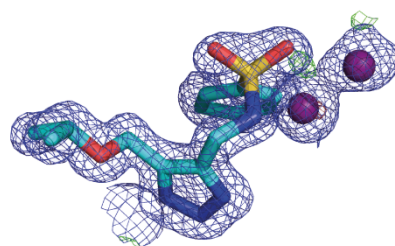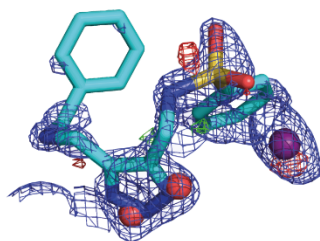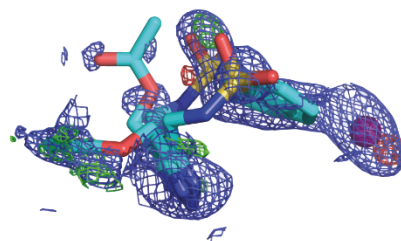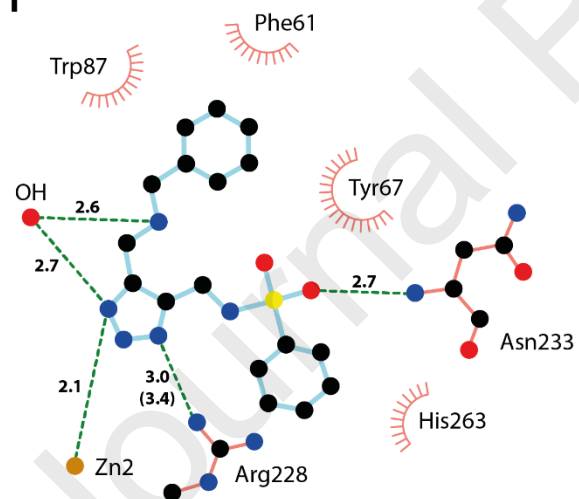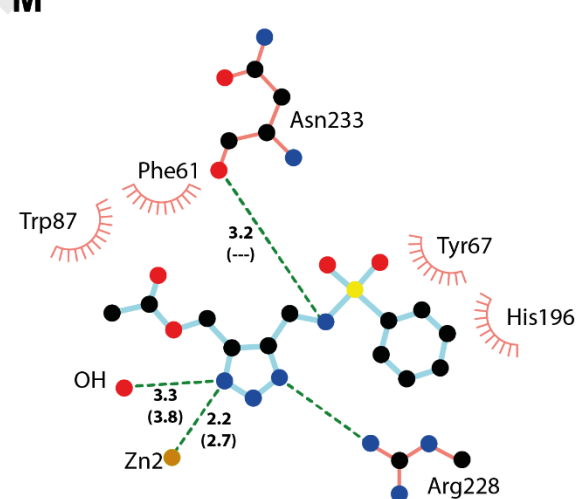
Figure 2. Final elections density maps (A, D, G and K), crystal structures (B, E, H and L) and interaction plots (C, F, I and M) for the inhibitor **1cc'** (A, B and C), **1dh'** (D, E, and F), **1di'** (G, H and I) and **1dj'** (K, L and M). The $2F_0$-F_C maps are shown in blue at 1.0σ for **1cc'** and **1dh'** and at 0.9σ for **1di'** and **1dj'**. The F_C-F_0 maps are shown at 4σ (green) and -4σ (red). In the crystal structures, carbon atoms of the inhibitors are depicted in cyan and protein carbon atoms in salmon. For the interaction plots, crystal structures were analysed using LIGPLOT [33]. Hydrogen bonds are shown as gre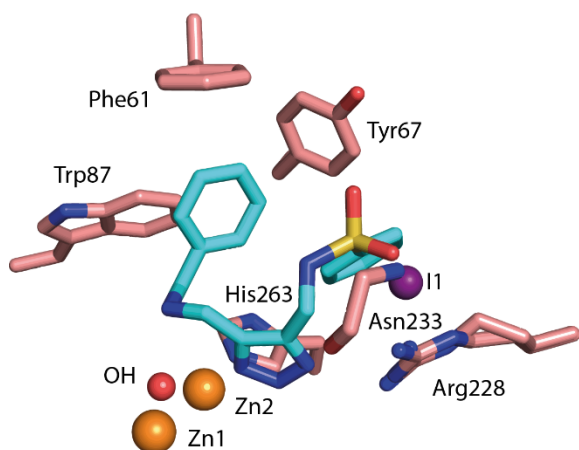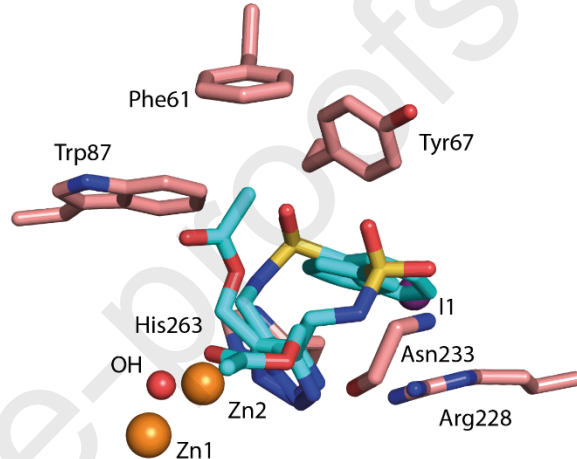en dashed lines and hydrophobic interactions by red arcs. All distances are given in Å. Distances for alternative conformation are given in brackets. For inhibitor **1dj'**, the figures are only shown for the VIM-2 molecule with higher ligand occupancy. In panel G, two water molecules are shown (red sphere), which are assumed to be artefacts from the native structure without bound ligand.

4   Materials and Methods

4.1 *Organic Synthesis*

All reagents and solvents were purchased from commercial sources and used as supplied unless otherwise stated. Compounds **3a**, **3c**, **3d**, **4a**, **4c**, **4d**, **1cc'**, **1cd'**, **1dg'** and **1dh'** were prepared according to the literature.[13] Reactions were monitored by thin-layer chromatography (TLC) with Merck pre-coated silica gel plates (60 F$_{254}$). Visualization was accomplished with either UV light or by immersion in potassium permanganate or phosphomolybdic acid (PMA) followed by light heating with a heating gun. Purification of reactions was carried out by flash column chromatography using silica gel from Merck (Silica gel 60, 0.040 - 0.063 mm). Purity analysis was carried out on Waters Acquity UPLC® BEH C18 (1.7 µm, 2.1 × 100 mm) column on a Waters Acquity I-class UPLC with Photodiode Array Detector. NMR spectra were obtained on a 400 MHz Bruker Avance III HD equipped with a 5 mm SmartProbe BB/1H (BB = 19F, 31P-15N). Data are represented as follows: chemical shift, multiplicity (s = singlet, d = doublet, t = triplet, q = quartet, m = multiplet), coupling constant (J, Hz) and integration. Chemical shifts (δ) are reported in ppm relative to the residual solvent peak (CDCl$_3$: $δ_H$ 7.26 and $δ_C$ 77.16; Methanol-d$_4$: $δ_H$ 3.31 and $δ_C$ 49.00). Positive ion electrospray ionization mass spectrometry was conducted on a Thermo electron LTQ Orbitrap XL spectrometer.

4.1.1   Synthesis of the sulfonamide derivatives from the corresponding sulfonylchlorides

The sulfonamides were prepared following the a procedure described by Weide *et al.*[13]

N-(4-chlorobut-2-ynyl)benzenesulfonamide (3a)[13]

Benzenesulfonylchloride (500 mg, 2.8 mmol, 1.0 equiv), 4-chlorobut-2-yn-1-amine hydrochloride **2** (515.26 mg, 3.68 mmol, 1.3 equiv), and K$_2$CO$_3$ (1.161 g, 8.4 mmol, 3.0 equiv), in THF/H$_2$O (14 mL, 1:1) gave compound **3a** (650 mg, 72%) as a colorless solid. R$_f$ = 0.37 (hexane/ethyl acetate, 65:35). Analytical data were in accordance with literature.[13] ^{1}H NMR (400 MHz, CDCl$_3$) δ 8.00 − 7.87 (m, 2H), 7.70 − 7.50 (m, 3H), 3.95 (t, J = 2.1 Hz, 2H), 3.89 (t, J = 2.1 Hz, 2H). ^{13}C NMR (101 MHz, CDCl$_3$) δ 139.4, 132.8, 128.9, 127.2, 80.3, 79.4, 77.2, 32.9, 29.6. HRMS (ESI): Calcd. for C$_{10}$H$_{10}$O$_2$NClNaS [M+H]$^+$ 266.0012; found 266.0013.

N-(4-chlorobut-2-ynyl)-4-methylbenzenesulfonamide (3b)

Toluene-4-sulfonylchloride (500 mg, 1.9 mmol, 1.0 equiv), 4-chlorobut-2-yn-1-amine hydrochloride **2** (477.42 mg, 2.50 mmol, 1.3 equiv), and K$_2$CO$_3$ (1.087 g, 7.5 mmol, 3.0 equiv), in THF/H$_2$O (12 mL, 1:1) gave compound **3c** (550 mg, 85%) as a colorless solid. R$_f$ = 0.46 (hexane/ethyl acetate, 35:65). **^{1}H NMR** (400 MHz, CDCl$_3$): δ 7.77 (d, J = 8.3 Hz, 2H), 7.32 (d, J = 8.0 Hz, 2H), 3.88 (d, J = 2.1 Hz, 4H), 2.43 (s, 3H).

320 **¹³C NMR** (101 MHz, CDCl₃): δ 143.9, 136.6, 129.7, 129.5, 127.5, 80.7, 79.5, 33.1, 29.9, 29.4, 21.6. **HRMS**

321 **(ESI)**: Calcd. for $C_{11}H_{12}O_2NClNaS$ [M+H]⁺ 280.0169; found 280.0169.

322 *2,5-dichloro-N-(4-chlorobut-2-ynyl)benzenesulfonamide (3c)[13]*

323 2,5-Dichlorobenzenesulfonylchloride (1000 mg, 4.1 mmol, 1.0 equiv), 4-chlorobut-2-yn-1-amine

324 hydrochloride **2** (741.4 mg, 5.3 mmol, 1.3 equiv), and K_2CO_3 (1.687 g, 12.21 mmol, 3.0 equiv), in

325 THF/H_2O (21 mL, 1:1) gave compound **3d** (1.084 mg, 87%) as a colorless solid. R_f = 0.40 (hexane/ethyl

326 acetate, 35:65). Analytical data were in accordance with literature.[13] **¹H NMR** (400 MHz, CDCl₃): δ 8.09

327 (d, *J* = 2.2 Hz, 1H), 7.52 – 7.48 (m, 2H), 5.33 (t, *J* = 6.5 Hz, 1H), 3.96 (d, *J* = 6.3 Hz, 2H), 3.82 (s, 2H). **¹³C**

328 **NMR** (101 MHz, CDCl₃): δ 138.6, 133.6, 133.3, 132.4, 130.9, 129.8, 79.7, 79.4, 77.2, 33.1, 29.3. **HRMS**

329 **(ESI)**: Calcd. for $C_{10}H_8O_2NCl_3S$ [M-H]⁻ 311.9233; found 311.9230.

330 *4-Iodo-N-(4-chlorobut-2-ynyl)-benzenesulfonamide (3d)[13]*

331 4-Iodobenzensulfonylchloride (1000 mg, 3.3 mmol, 1.0 equiv), 4-chlorobut-2-yn-1-amine

332 hydrochloride **2** (602 mg, 4.3 mmol, 1.3 equiv), and K_2CO_3 (1.368 g, 9.9 mmol, 3.0 equiv), in THF/H_2O

333 (18 mL, 1:1) gave compound **3e** (880 mg, 72%) as a colorless solid. R_f = 0.41 (hexane/ethyl acetate,

334 35:65). **¹H NMR** (400 MHz, CDCl₃): δ 7.96 – 7.83 (m, 2H), 7.61 (d, *J* = 8.6 Hz, 2H), 4.67 (s, 1H), 4.01 –

335 3.76 (m, 4H). **¹³C NMR** (101 MHz, CDCl₃): δ 176.2, 139.5, 138.4, 128.8, 100.5, 80.3, 79.8, 33.1, 29.7.

336 **HRMS (ESI)**: Calcd. for $C_{10}H_8O_2NClIS$ [M-H]⁻ 367.9022; found 367.9003.

337 ### 4.1.2   Synthesis of the azide derivatives from the corresponding chlorides

338 The azides were prepared following modified procedure based on Weide *et al.*[13]

339 *N-(4-azidobut-2-ynyl)benzenesulfonamide (4a)*

340 *N*-(4-chlorobut-2-ynyl)benzenesulfonamide (**3a**) (100 mg, 0.41 mmol, 1.0 equiv), sodium azide (31.98

341 mg, 0.492 mmol, 1.2 equiv), and NH_4Cl (5.5 mg, 0.1 mmol, 0.25 equiv), in DMF (5 mL) gave compound

342 **4a** (66.3 mg, 66%) as a colorless solid. R_f = 0.33 (hexane/ethyl acetate, 65:35). **¹H NMR** (400 MHz,

343 CDCl₃): δ 7.91 (d, J = 7.0 Hz, 2H), 7.66 – 7.46 (m, 3H), 5.12 (s, 1H), 3.92 (s, 2H), 3.64 (s, 2H). **¹³C NMR**

344 (101 MHz, CDCl₃): δ 139.5, 132.7, 128.9, 127.1, 81.2, 76.9, 39.4, 32.8. **HRMS (ESI)**: Calcd. for

345 $C_{10}H_{10}O_2N4NaS$ [M+Na]⁺ 273.0419; found 273.0417.

346 *N-(4-azidobut-2-ynyl)-4-methylbenzenesulfonamide (4b)*

347 *N*-(4-chlorobut-2-ynyl)-4-methylbenzenesulfonamide (**3b**) (100 mg, 0.39 mmol, 1.0 equiv), sodium

348 azide (30.0 mg, 0.47 mmol, 1.2 equiv), and NH_4Cl (5.2 mg, 0.09 mmol, 0.25 equiv), in DMF (5 mL) gave

349 compound **4b** (80 mg, 84%) as a colorless solid. R_f = 0.43 (hexane/ethyl acetate, 65:35). **¹H NMR** (400

350 MHz, CDCl₃): δ 7.78 (d, *J* = 8.3 Hz, 2H), 7.31 (d, *J* = 8.0 Hz, 2H), 5.03 (t, *J* = 5.8 Hz, 1H), 3.89 (d, *J* = 6.1 Hz,

351 2H), 3.67 (s, 2H), 2.42 (s, 3H). ^{13}**C NMR** (101 MHz, CDCl$_3$): δ 144.3, 137.0, 130.1, 127.8, 82.0, 77.4, 40.1,

352 33.4, 21.9. **HRMS (ESI)**: Calcd. for C$_{11}$H$_{12}$O$_2$N$_4$NaS [M+Na]$^+$ 287.0576; found 287.0573.

353 *N-(4-azidobut-2-ynyl)-2,5-dichlorobenzenesulfonamide (4c)*

354 2,5-Dichloro-*N*-(4-chlorobut-2-ynyl)benzenesulfonamide **3c** (1000 mg, 3.2 mmol, 1.0 equiv), sodium

355 azide (250.8 mg, 3.85 mmol, 1.2 equiv), and NH$_4$Cl (42.4 mg, 0.8 mmol, 0.25 equiv), in DMF (49 mL)

356 gave compound **4c** (980 mg, 96%) was obtained as a colorless solid. R$_f$ = 0.41 (hexane/ethyl acetate,

357 65:35). ^{1}**H NMR** (400 MHz, CDCl$_3$): δ 8.09 (d, *J* = 2.2 Hz, 1H), 7.48 (s, 2H), 5.43 (t, *J* = 6.2 Hz, 1H), 3.97

358 (dd, *J* = 6.3, 0.7 Hz, 2H), 3.63 (t, *J* = 2.0 Hz, 2H). ^{13}**C NMR** (101 MHz, CDCl$_3$): δ 138.9, 133.92, 133.90,

359 133.6, 132.6, 131.2, 130.1, 80.6, 77.5, 77.2, 39.6, 33.2. **HRMS (ESI)**: Calcd. for C$_{10}$H$_7$N$_4$O$_2$Cl$_2$S [M-H]$^-$

360 316.9670; found 316.9661.

361 *N-(4-azidobut-2-ynyl)-4-iodobenzenesulfonamide (4d)*

362 *N*-(4-chlorobut-2-ynyl)-4-iodobenzenesulfonamide **3d** (850 mg, 2.3 mmol, 1.0 equiv), sodium azide

363 (179.7 mg, 2.76 mmol, 1.2 equiv), and NH$_4$Cl (36.6 mg, 0.69 mmol, 0.25 equiv), in DMF (30 mL) gave

364 compound **4d** (780 mg, 90%) was obtained as a colorless solid. R$_f$ = 0.37 (hexane/ethyl acetate, 65:35).

365 ^{1}**H NMR** (400 MHz, CDCl$_3$): δ 7.88 (d, *J* = 8.5 Hz, 2H), 7.61 (d, *J* = 8.5 Hz, 2H), 5.19 (s, 1H), 3.92 (s, 2H),

366 3.68 (d, *J* = 2.0 Hz, 2H). ^{13}**C NMR** (101 MHz, CDCl$_3$): δ 139.5, 138.46, 138.45, 138.4, 128.9, 128.8, 100.6,

367 81.3, 77.4, 77.2, 39.8, 33.1. **HRMS (ESI)**: Calcd. for C$_{10}$H$_9$IN$_4$O$_2$S [M-H]$^-$ 374.9412; found 374.9407.

368 ### 4.1.3 General Procedure for the synthesis of *N*H-triazole-arylsulfonamides

369 To azide **4a–d** (1 equiv) as solution in CH$_2$Cl$_2$ or neat was added the nucleophile (1-5 equiv.). The

370 reaction mixture was stirred at 60 °C for 16 h. The reaction was concentrated under reduced pressure

371 to give the crude product. All triazoles were purified by flash column chromatography on silica gel (50–

372 100% EtOAc in hexanes to 10% MeOH in EtOAc). Repeated column chromatography provided most

373 compounds with purity greater than 90% as determined by HPLC.

374 *N-((5-(aminomethyl)-1H-1,2,3-triazol-4-yl)methyl)benzenesulfonamide (1aa')*

375 *N*-(4-azidobut-2-ynyl)benzenesulfonamide **4a** (68 mg, 0.27 mmol, 1.0 equiv) and ammonium hydroxide

376 solution (28% NH$_3$ in H$_2$O, 2 mL) gave **1aa'** (47 mg, 65%) as a pale yellow oil. ^{1}**H NMR** (400 MHz, DMSO-

377 *d*$_6$): δ 7.79 (s, 2H), 7.71 − 7.38 (m, 3H), 4.06 (s, 2H), 3.70 (s, 2H). ^{13}**C NMR** (101 MHz, DMSO-*d*$_6$): δ 143.3,

378 140.6, 139.2, 132.8, 129.5, 129.5, 126.9, 37.7, 35.6. **HRMS (ESI)**: Calcd. for C$_{10}$H$_{14}$O$_2$N$_5$S [M+H]$^+$

379 268.0862; found 268.0863. **HPLC purity**: 91%

380 *N-((5-(tert-butoxymethyl)-1H-1,2,3-triazol-4-yl)methyl)-4-methylbenzenesulfonamide (1bb')*

381 *N*-(4-azidobut-2-ynyl)-4-methylbenzenesulfonamide **4b** (66 mg, 0.25 mmol, 1.0 equiv) in CH$_2$Cl$_2$ (2 mL)

382 and 2-methyl-2-propanol (74 mg, 1.0 mmol, 4.0 equiv) gave **1bb'** (55 mg, 65%) as colorless oil. ^{1}**H NMR**

383 (400 MHz, CD$_3$OD): δ 7.69 (d, J = 8.2 Hz, 2H), 7.34 (d, J = 8.2 Hz, 2H), 4.50 (s, 2H), 4.18 (s, 2H), 2.42 (s,

384 3H), 1.26 (s, 9H). **^{13}C NMR** (101 MHz, CD$_3$OD): δ 144.8, 144.2 (determined from HMBC), 143.8

385 (determined from HMBC), 138.5, 130.7, 128.2, 75.5, 56.2, 38.6, 27.7, 21.4. **HRMS (ESI)**: Calcd. for

386 C$_{15}$H$_{22}$O$_3$N$_4$NaS [M+Na]$^+$ 361.1300; found 361.1305. **HPLC purity**: 87%

387 *N-((5-((cyclohexylamino)methyl)-1H-1,2,3-triazol-4-yl)methyl)-4-methylbenzenesulfonamide (1bc')*

388 *N*-(4-azidobut-2-yny)-4-methylbenzenesulfonamide **4b** (78 mg, 0.29 mmol, 1.0 equiv) and

389 cyclohexylamine (115 mg, 1.16 mmol, 4.0 equiv) gave **1bc'** (75 mg, 71%) as colorless solid. **^{1}H NMR**

390 (400 MHz, CD$_3$OD) δ 7.78 – 7.69 (m, 2H), 7.43 – 7.34 (m, 2H), 4.15 (s, 2H), 3.98 (s, 2H), 2.72 – 2.60 (m,

391 1H), 2.43 (s, 3H), 2.07 – 1.98 (m, 2H), 1.84 – 1.75 (m, 2H), 1.71 – 1.63 (m, 1H), 1.38 – 1.12 (m, 5H). **^{13}C**

392 **NMR** (101 MHz, CD$_3$OD) δ 144.9, 140.9, 140.1, 138.4, 130.8, 128.2, 57.4, 40.3, 38.7, 32.6, 26.8, 25.9,

393 21.5. **HRMS (ESI)**: Calcd. for C$_{17}$H$_{26}$O$_2$N$_5$S [M+H]$^+$ 364.1798; found 364.1802.

394 *N-((5-((adamantylamino)methyl)-1H-1,2,3-triazol-4-yl)methyl)-4-methylbenzenesulfonamide (1bd')*

395 *N*-(4-azidobut-2-ynyl)-4-methylbenzenesulfonamide **4b** (20 mg, 0.07 mmol, 1.0 equiv) in CH$_2$Cl$_2$ (2 mL)

396 and 1-adamantylamine (34.2 mg, 0.226 mmol, 3.0 equiv) gave **1bd'** (24 mg, 83%) as colorless solid. **^{1}H**

397 **NMR** (400 MHz, CD$_3$OD) δ 7.75 – 7.68 (m, 2H), 7.39 – 7.33 (m, 2H), 4.14 (s, 2H), 4.01 (s, 2H), 2.41 (s,

398 3H), 2.17 – 2.11 (m, 3H), 1.85 (d, J = 2.9 Hz, 6H), 1.79 – 1.66 (m, 6H). **^{13}C NMR** (101 MHz, CD$_3$OD) δ

399 144.9, 141.0, 139.5, 138.3, 130.8, 128.1, 55.6, 41.1, 38.7, 37.1, 35.2, 30.8, 21.5. **HRMS (ESI)**: Calcd. for

400 C$_{21}$H$_{28}$O$_2$N$_5$S [M-H]$^-$ 414.1970; found 414.1965. **HPLC purity**: 89%

401 *2,5-Dichloro-N-((5-((cyclohexylamino)methyl)-1H-1,2,3-triazol-4-yl)methyl)benzenesulfonamide (1cc')[13]*

402 *N*-(4-azidobut-2-ynyl)-2,5-dichlorobenzenesulfonamide **4c** (93 mg, 0.29 mmol, 1.0 equiv) in CH$_2$Cl$_2$ (4

403 mL) and cyclohexylamine (86.1 mg, 0.87 mmol, 3 equiv) gave **1cc'** (88 mg, 72%) as colorless solid. **^{1}H**

404 **NMR** (400 MHz, CD$_3$OD): δ 7.96 (d, J = 2.4 Hz, 1H), 7.57 (dd$_{AB}$, J = 8.5, 2.4 Hz, 1H), 7.53 (d$_{AB}$, J = 8.5 Hz,

405 1H), 4.27 (s, 2H), 3.99 (s, 2H), 2.74 – 2.62 (m, 1H), 2.05 – 2.02 (m, 2H), 1.82 – 1.78 (m, 2H), 1.69 – 1.65

406 (m, J = 12.5 Hz, 1H), 1.37 – 1.16 (m, 5H). **^{13}C NMR** (101 MHz, CD$_3$OD): δ 140.8, 140.7, 140.1, 134.6,

407 134.3, 134.1, 131.7, 131.3, 57.5, 40.2, 38.3, 32.6, 26.8, 25.9. **HRMS (ESI)**: Calcd. for C$_{16}$H$_{22}$O$_2$N$_5$Cl$_2$S

408 [M+H]$^+$ 418.0861; found 418.0866. **HPLC purity**: 95%

409 *2,5-Dichloro-N-((5-((adamantylamino)methyl)-1H-1,2,3-triazol-4-yl)methyl)benzenesulfonamide*

410 *(1cd')[13]*

411 *N*-(4-azidobut-2-ynyl)-2,5-dichlorobenzenesulfonamide **4c** (102 mg, 0.32 mmol, 1.0 equiv), 1-

412 adamentylamine (58.2 mg, 0.38 mmol, 1.2 equiv) in CH$_2$Cl$_2$ (4 mL) gave **1cd'** (111 mg, 73%) as colorless

413 solid. **^{1}H NMR** (400 MHz, CD$_3$OD) δ 8.00 – 7.95 (m, 1H), 7.62 – 7.51 (m, 2H), 4.28 (s, 2H), 3.97 (s, 2H),

414 2.16 (s, 3H), 1.86 (d, J = 2.9 Hz, 6H), 1.82 – 1.69 (m, 6H). **^{13}C NMR** (101 MHz, CD$_3$OD) δ 140.9, 140.6,

415   140.1, 134.6, 134.3, 134.2, 131.7, 131.3, 54.7, 41.6, 38.4, 37.3, 35.2, 30.9. **HRMS (ESI)**: Calcd. for

416     $C_{20}H_{26}O_2N_5ClS$ [M+H]$^+$ 470.1182; found 470.1179. **HPLC purity**: 94%

417   *N-((5-((cyclohexylamino)methyl)-1H-1,2,3-triazol-4-yl)methyl)-4-iodobenzenesulfonamide (1dc')*

418   *N*-(4-azidobut-2-ynyl)-4-iodobenzenesulfonamide **4d** (86 mg, 0.228 mmol, 1.0 equiv), cyclohexylamine

419   (83.9 mg, 0.845 mmol, 4.0 equiv) in CH_2Cl_2 (2 mL) gave **1dc'** (99 mg, 86%) as colorless oil. **¹H NMR** (400

420   MHz, $CDCl_3$): δ 7.82 (d, *J* = 8.1 Hz, 2H), 7.56 (d, *J* = 8.1 Hz, 2H), 4.08 (s, 2H), 3.99 (s, 2H), 2.80 (s, 1H),

421   2.13 – 2.01 (m, 2H), 1.76 (d, *J* = 7.1 Hz, 2H), 1.64 (d, *J* = 12.4 Hz, 1H), 1.34 – 1.11 (m, 6H). **¹³C NMR** (101

422   MHz, $CDCl_3$): δ 139.9, 139.6, 138.3, 136.5, 128.5, 99.8, 57.5, 39.8, 38.4, 31.5, 25.5, 24.9. **HRMS (ESI)**:

423   Calcd. for $C_{16}H_{23}O_2N_5SI$ [M+H]$^+$ 476.0612; found 476.0612. **HPLC purity**: 99%

424   *N-((5-((adamantylamino)methyl)-1H-1,2,3-triazol-4-yl)methyl)-4-iodobenzenesulfonamide (1dd')*

425   *N*-(4-azidobut-2-ynyl)-4-iodobenzenesulfonamide **4d** (77 mg, 0.20 mmol, 1.0 equiv), 1-

426   adamantylamine (37.2 mg, 0.226 mmol, 1.2 equiv) in CH_2Cl_2 (4 mL) gave **1dd'** (102 mg, 96%) as colorless

427   solid. **¹H NMR** (400 MHz, DMSO-d$_6$): δ 8.01 – 7.89 (m, 2H), 7.55 – 7.50 (m, 2H), 5.78 – 5.73 (m, 1H),

428   4.14 – 4.05 (m, 2H), 3.70 – 3.63 (m, 2H), 3.23 – 3.12 (m, 1H), 2.00 (s, 3H), 1.65 – 1.48 (m, 12H). **¹³C NMR**

429   (101 MHz, DMSO-d$_6$): δ δ 142.2 (determined by HMBC), 139.9, 139.3 (determined by HMBC), 138.0,

430   128.3, 100.4, 50.4, 41.5, 37.6, 36.2, 34.2, 28.9. **HRMS (ESI)**: Calcd. for $C_{20}H_{27}O_2N_5SI$ [M+H]$^+$ 528.0925;

431   found 528.0925. **HPLC purity**: 97%

432   *N-((5-((tritylamino)methyl)-1H-1,2,3-triazol-4-yl)methyl)-4-iodo-benzenesulfonamide (1de')*

433   *N*-(4-azidobut-2-ynyl)-4-iodobenzenesulfonamide **4d** (100 mg, 0.26 mmol, 1.0 equiv) in CH_2Cl_2 (5 mL)

434   and triphenylmethanamine (82.2 mg, 0.319 mmol, 1.2 equiv) gave **1de'** (63 mg, 93%) as colorless solid.

435   **¹H NMR** (400 MHz, $CDCl_3$): δ 7.69 (d, *J* = 8.2 Hz, 2H), 7.43 (d, *J* = 8.1 Hz, 5H), 7.37 – 7.20 (m, 12H), 4.25

436   (s, 2H), 3.42 (s, 2H). **¹³C NMR** (101 MHz, $CDCl_3$): δ 145.0, 139.6, 138.4, 128.7, 128.6, 128.31, 128.27,

437   128.1, 127.0, 100.1, 71.4, 38.4, 37.8. **HRMS (ESI)**: Calcd. for $C_{29}H_{26}O_2N_5SI$ [M+Na]$^+$ 658.0748; found

438   658.0744. **HPLC purity**: 81%

439   *N-((5-((4-methoxybenzylthio)methyl)-1H-1,2,3-triazol-4-yl)methyl)-4-iodo-benzenesulfonamide (1df')*

440   *N*-(4-azidobut-2-ynyl)-4-iodobenzenesulfonamide **4d** (80 mg, 0.21 mmol, 1.0 equiv) in CH_2Cl_2 (5 mL)

441   and 4-methoxybenzyl mercaptan (161.9 mg, 1.05 mmol, 5 equiv) gave **1df'** (70 mg, 63%) as dark brown

442   oil. **¹H NMR** (400 MHz, $CDCl_3$): δ 7.77 (d, *J* = 8.5 Hz, 2H), 7.50 (d, *J* = 8.4 Hz, 2H), 7.17 (d, *J* = 8.5 Hz, 2H),

443   6.81 (d, *J* = 8.5 Hz, 2H), 6.35 (s, 1H), 4.22 (s, 2H), 3.77 (s, 3H), 3.60 (s, 2H), 3.55 (s, 2H). **¹³C NMR** (101

444   MHz, CD_3OD): δ 160.2, 141.7 (determined by HMBC), 141.4, 140.4 (determined by HMBC), 139.5,

445   131.1, 129.6, 114.9, 100.5, 55.7, 38.3, 36.2, 25.1. **HRMS (ESI)**: Calcd. for $C_{18}H_{18}O_3N_4IS_2$ [M-H]$^-$ 528.9876;

446   found 528.9835. **HPLC purity**: 96%

447 *4-Iodo-N-((5-(methoxymethyl)-1H-1,2,3-triazol-4-yl)methyl)benzenesulfonamide (1dg')[14]*

448 *N*-(4-azidobut-2-ynyl)-4-iodobenzenesulfonamide **4d** (106 mg, 0.28 mmol, 1.0 equiv) in methanol (2

449 mL) gave **1dg'** (101 mg, 88%) as colorless oil. **^{1}H NMR** (400 MHz, CD$_3$OD) δ 7.90 (d, *J* = 8.5 Hz, 2H), 7.54

450 (d, *J* = 8.5 Hz, 2H), 4.48 (s, 2H), 4.22 (s, 2H), 3.33 (s, 3H). **^{13}C NMR** (101 MHz, CD$_3$OD) δ 143.1 (determined

451 from HMBC), 142.7 (determined from HMBC), 141.5, 139.5, 129.6, 100.4, 65.5, 58.7, 38.1. **HRMS (ESI)**:

452 Calcd. for C$_{11}$H$_{13}$O$_3$N$_4$IS [M+H]$^+$ 409.9861; found 409.9848. **HPLC purity**: 98%

453 *4-Iodo-N-((5-(isopropoxymethyl)-1H-1,2,3-triazol-4-yl)methyl)benzenesulfonamide (1dh')[13]*

454 *N*-(4-azidobut-2-ynyl)-4-iodobenzenesulfonamide **4d** (80 mg, 0.212 mmol, 1.0 equiv), in isopropanol (2

455 mL) gave **1dh'** (99 mg, 86%) as colorless oil. **^{1}H NMR** (400 MHz, CD$_3$OD): δ 7.95 – 7.89 (m, 3H), 7.55 (d,

456 *J* = 8.1 Hz, 2H), 4.55 (s, 2H), 4.23 (s, 2H), 3.76 – 3.61 (m, 1H), 1.18 (d, *J* = 6.1 Hz, 6H). **^{13}C NMR** (101 MHz,

457 CD$_3$OD): δ 141.4, 140.8 (2 × triazole C, determined from HMBC), 139.5, 129.6, 100.5, 73.2, 60.9, 49.0,

458 38.0, 22.2. **HRMS (ESI)**: Calcd. for C$_{13}$H$_{17}$O$_3$N$_4$SINa [M+Na]$^+$ 458.9958; found 458.9958. **HPLC purity**:

459 95%

460 *N-((5-((benzylamino)methyl)-1H-1,2,3-triazol-4-yl)methyl)-4-iodobenzenesulfonamide (1di')*

461 *N*-(4-azidobut-2-ynyl)-4-iodobenzenesulfonamide **4d** (100 mg, 0.26 mmol, 1.0 equiv),

462 phenylmethanamine (139.0 mg, 1.3 mmol, 3 equiv) in CH$_2$Cl$_2$ (5 mL) gave **1di'** (95 mg, 72%) as colorless

463 oil. **^{1}H NMR** (400 MHz, CDCl$_3$): δ 7.74 (d, J = 8.4 Hz, 2H), 7.46 (d, J = 8.4 Hz, 2H), 7.39 – 7.26 (m, 5H),

464 4.15 (s, 2H), 3.86 (d, J = 8.2 Hz, 4H). **^{13}C NMR** (101 MHz, CDCl$_3$): δ 140.9 (triazole, determined by HMBC),

465 140.6 (triazole, determined by HMBC), 139.7, 138.4, 137.1, 128.9, 128.6, 128.1, 100.0, 53.1, 42.5, 38.1.

466 **HRMS (ESI)**: Calcd. for C$_{20}$H$_{23}$O$_2$N$_2$IS [M-H]$^-$ 482.0146; found 482.0519.

467 *(4-((4-iodophenylsulfonamido)methyl)-1H-1,2,3-triazol-5-yl)methyl acetate (1dj')*

468 N-(4-azidobut-2-ynyl)-4-iodobenzenesulfonamide **4d** (300 mg, 0.80 mmol, 1.0 equiv) and H$_2$O (2 mL)

469 were heated at 60°C overnight. The reaction mixture was evaporated to yield crude 5-hydroxymethyl

470 triazole. A small portion of the crude was taken and acylated as follows. 5-Hydroxymethyl triazole (50

471 mg, 0.13 mmol, 1.0 equiv), Et$_3$N (55 μL, 0.39 mmol, 3.0 equiv), DMAP (1.5 mg, 0.013 mmol, 10 mol%)

472 and acetic anhydride (12 μL, 0.13 mmol,1.0 equiv) were stirred in CH$_2$Cl$_2$ (20 mL/mmol of triazole) for

473 15–30 min (reaction was monitored by TLC). The reaction mixture was evaporated and purified by

474 column chromatography to yield **1dj'** (31mg, 54%) as colorless solid. **^{1}H NMR** (400 MHz, CD$_3$OD): δ 7.98

475 – 7.84 (m, 2H), 7.62 – 7.49 (m, 2H), 5.12 (s, 2H), 4.24 (s, 2H), 2.04 (s, 3H). **^{13}C NMR** (101 MHz, CD$_3$OD):

476 δ 172.3, 141.5 (2*C; triazole, determined by HMBC), 140.8 (triazole, determined by HMBC), 139.5,

477 129.5, 100.5, 57.1, 37.9, 20.6. **HRMS (ESI)**: Calcd. for C$_{12}$H$_{14}$O$_4$N$_4$SI [M+H]$^+$ 436.9775; found 436.9775.

478 **HPLC purity**: 89%

479 *4.2 Biological activity*

480 ### 4.2.1 Gene Constructs of VIM-2, NDM-1 and GIM-1

481 In this study two types of gene constructs were used. The first included the native leader sequence to

482 allow the proteins to be transported to the periplasm, for the three enzymes VIM-2 from *Pseudomonas*

483 *aeruginosa strain 301-5473 (*GenBank no Q9K2N0*)*, GIM-1 from *P. aeruginosa* (GenBank no Q704V1;

484 [19, 34]) and NDM-1 (GenBank no. E9NWK5, e.g [35, 36]), where the latter bla_{NDM-1} gene is reported from

485 several organisms. Cloning of bla_{NDM-1} or bla_{GIM-1} genes into the *Escherichia coli* pET26b(+) vector

486 (Novagen) was performed using the Primers listed in **Table S3**, and by restriction cutting as described

487 for VIM-26.[37] Cloning of bla_{VIM-2} into pET26b(+) is described previously.[38] The obtained *E. coli* pET-

488 26b(+) MBL constructs were further used in the in the whole cell-based inhibitor assays.

489 In the second set of gene constructs used for the recombinant gene expression, the native leader

490 sequence was removed and replaced with a hexa-His tag and a TEV cleavage site as reported earlier

491 for VIM-2 (residues V27-E268;[17]) and GIM-1 (residues Q19-D250;[19]) both in pDEST14. NDM-1 used a

492 codon optimized synthetic gene (Life Technologies, Thermo Fisher Scientific), with a TEV cleavage site

493 with sequence ENLYFQG and residues G36-R280 in NDM-1 transformed in pDONR™221, and further

494 sub cloned into pDEST17 with carries an N-terminal hexa His-tag, yielding pDest17-NDM-1 construct.

495 Herein the residue numbering is the class B β-lactamase numbering scheme will be applied.[39]

496 ### 4.2.2 Recombinant protein expression and purification of VIM-2, GIM-1 and NDM-1

497 The proteins were expressed and purified following this protocol. pDest17-NDM-1 was transformed

498 into *E. coli* BL21 Star (DE3) pLysS (Invitrogen), and pDEST14 plasmids with VIM-2 or GIM-1 were

499 transformed into in-house modified *E. coli* BL21 Star (DE3) pLysS (Invitrogen) cells with the pRARE

500 plasmid (Novagen) in order to allow expression of genes encoding tRNAs for rare codons.[40] Precultures

501 grown in Terrific Broth (TB) media with 100 μg/ml ampicillin (Sigma-Aldrich) and 34 μg/ml

502 chloramphenicol (Sigma-Aldrich). The precultures were inoculated to 2 L Luria-Bertani (LB) media

503 containing 100 μg/ml ampicillin and 34 μg/ml chloramphenicol and grown at 37 °C to reach an optical

504 density (OD_{600} nm) of 0.5-1.0 before induced expression with 0.4 mM isopropyl β-D-1-

505 thigalactopyranoside (IPTG; Sigma-Aldrich). The induced cultures were grown overnight at 20°C before

506 collecting the cells by centrifugation (8,900 X g, 30 min, 4 °C). Buffer A containing 50 mM HEPES pH

507 7.2, 100 μM $ZnCl_2$ and 150 mM NaCl was used to resuspend the cell pellets, following sonication and

508 collecting the supernatants by centrifugation (3000 g, 40 min, 4°C). The recombinant proteins were

509 affinity purified using a 1 ml or 5 ml His-Trap HP column (GE Healthcare) in buffer A washed with 5%

510 buffer B (50 mM HEPES pH 7.2, 100 μM $ZnCl_2$, 150 mM NaCl and 1 M imidazole), before eluted in a

511 gradient of 5 to 100 % buffer B. Peak fractions were investigated using 4-20% sodium dodecyl sulfate

512   polyacrylamide gel electrophoresis (SDS-PAGE; Bio-Rad) [41]. The fractions containing MBL protein was

513   added in-house-made His-tagged TEV protease in a 1:100 mg ratio of TEV:protein and dialyzed at 4 °C

514   overnight using 10-kDa cutoff Snakeskin (Pierce) in buffer C (50 mM HEPES pH 7.2, 150 mM NaCl, 1

515   mM EDTA and 1 mM β-mercaptoethanol). To remove uncleaved protein and TEV protease a second

516   His-Trap purification was performed. SDS-PAGE analysis was used to estimate a purity of ~95% of the

517   fractions containing protein, which then were pooled and dialyzed in buffer A overnight.

4.2.3 Dose Rate Inhibition Studies for IC_{50} Determination

519   The half-maximal inhibitory concentration (IC_{50}) against the VIM-2, NDM-1 and GIM-1 enzymes were

520   determined by using sixteen different concentration of inhibitor compounds ranging from 0 µM to 250

521   µM. A 100 µl solution with 50 mM HEPES buffer (pH 7.2), 100 µM $ZnCl_2$), purified enzyme (1 nM VIM-

522   2, NDM-1 or GIM-1) and 2.5-0 mM inhibitor was incubated in a 96 well plate at 25 °C for 5 min. In

523   addition, the enzyme buffer contained 400 µg/ml Bovine Serum Albumin (BSA) to prevent protein

524   unfolding and loss of activity due to low concentrations [42, 43]. 100 µM of the reporter substrate

525   nitrocefin (VIM-2, GIM-1) or imipenem (NDM-1) was added to the enzyme-inhibitor solution and the

526   increase in absorbance at 482 nm (nitrocefin) or 300 nm (imipenem) was recorded on a Spectramax

527   M2e spectrophotometer (Molecular Devices). Each data point was performed in triplicates and the

528   initial velocity for each inhibitor concentration was analysed by a log [inhibitor] vs. response curve

529   fitting to calculate IC_{50} in GraphPad Prism 5.0 software.

4.2.4 Cell-based screening assay of the inhibition potential

531   The inhibitory activity of the inhibitors was investigated in a cell-based assay using a β-lactamase-

532   negative *E. coli* SNO3 (*ampA1 ampC8 pyrB recA rpsL*)[44] transformed with pET26b(+) containing *bla*_{VIM-}

533   2, *bla*_{GIM-1} or *bla*_{NDM-1}. The screen was conducted in 96-well plates (Corning) in duplicates. 50 µl

534   overnight culture (adjusted to an OD_{600} of 1 in LB broth) of *E. coli* SNO3 containing one of the MBLs,

535   inhibitor (with a final concentration of 250 µM), 0.8 mM (final concentration) Isopropyl ß-D-1-

536   thiogalactopyranoside (Sigma, IPTG) and 50 µl LB media, were added to each well. The plate was

537   incubated at 37 °C for 20 min with shaking to induce the expression of the MBL. Subsequently, 50 µl

538   nitrocefin (diluted in 50 mM HEPES pH 7.2 and 100 µM $ZnCl_2$ to give a final concentration of 1.6 mM in

539   the assay) was added. Nitrocefin hydrolysis was measured at OD_{482} every minute for 3 hours with

540   shaking (47 seconds) in between reads using a Spectramax M2^e spectrophotometer (Molecular

541   Devices). EDTA (250 µM concentration) was used as positive control and wells containing no inhibitor

542   as negative controls. The percent inhibition was calculated according to equation 1.

543

544 $\%\text{ inhibition} = \frac{\text{Slope (No inhibitor)} - \text{Slope (Inhibitor)}}{\text{Slope (No inhibitor)}} \times 100\%$ equation (1)

545

546 The synergistic effect of the inhibitors with meropenem was tested against selected clinical bacterial

547 strains containing MBLs. The bacterial strains were plated on lactose agar plates with 100 mg/L

548 ampicillin and lactose agar and incubated overnight at 37°C. The inhibitors were diluted to a final

549 concentration of 50 µM (**1cc'**, **1dj'**) or 125 µM (**1dc'**) in Mueller Hinton (MH) broth. In order to monitor

550 the effect of the DMSO in the assay, a DMSO control was included with a concentration of 5%.

551 Meropenem was diluted in MH broth in a 2-fold dilution series with final concentrations of 256 µg/mL

552 - 0.0625 µg/mL. The microtiter plates were inoculated with a 0.5 McFarland suspension of the bacterial

553 strain in 0.85% NaCl, which were diluted in MH broth. A quality check of bacterial suspension in 0.85%

554 NaCl in a 1:100 ratio was incubated on MH agar plates overnight at 37°C. The final CFU/mL inoculum

555 were calculated and compared to a standard. The microtiter plates were incubated for 20 hours at

556 37°C. The minimum inhibitory concentrations (MIC) were detected by visual inspection of the plates

557 the next day.

558 *4.3 Crystallization, X-ray data collection and data analysis*

559 The DMSO-free co-crystallization method[45] was used to crystallize VIM-2 in complex with the inhibitor

560 **1cc´, 1dh´** and **1di´**. In brief, the inhibitors were dissolved in DMSO and used to pre-coat the reservoir

561 wells of an MRC-96-well crystallization plate (Molecular Dimensions) by DMSO evaporating. Reservoir

562 solution consisting of 22-27% polyethylene glycol (PEG) 3350 and 0.2 M magnesium formate was

563 added to every well and incubated for 24 h. The reservoir solution was mixed with the protein solution

564 (9.4 mg/ml) in a 1:1 ratio and used for sitting-drop experiments. Protein crystals were harvested after

565 1-2 weeks.

566 Soaking of native VIM-2 crystals was used for the crystallization of VIM-2 in complex with the inhibitor

567 **1dj´** [17].The native VIM-2 crystals were grown using the hanging drop-method and reservoir solution

568 consisting of 22-27% PEG 3350 and 0.2 M magnesium formate. **1dj´** was dissolved in DMSO at a

569 concentration of 100 mM. The native VIM-2 crystals were transferred to reservoir solution containing

570 2.5 mM **1dj´** and harvested after 12 h.

571 After harvesting, all crystals were transferred to 25% PEG 3350, 0.2 M $MgCl_2$, 15% ethylene glycol, 50

572 mM HEPES pH 7.2 and flash cooled in liquid nitrogen. The collection of the X-ray data was carried out

573 at the ID23-1 or ID-29 at the European Synchrotron Radioation Facility (ESRF) in Grenoble, France. The

574 data sets were integrated, scaled and truncated using XDS [46], POINTLESS and AIMLESS [47, 48]. Molecular

575 replacement was carried out using PHASER [49] with a previously published VIM-2 structure (PDB:

576 1KO3)[28]. Several refinement cycles in PHENIX [50] and molecular modeling in WinCoot [51] according to the

577 2Fo-Fc and Fo-Fc map were used to obtain the final structure. For the complex structures with the

578 inhibitors **1dh´** and **1cc´**, all atoms except water were refined with anisotropic B-factors. For the

579 complex structures with **1di´** and **1dj´,** TLS parameters and anisotropic B-factors refinement for Zn^{2+}

580 and Cl^- were applied. R-free cross validation was done with 5% of the data. Conditions for the data

581 collection and refinement statistics are shown in Table 1. The PyMOL Molecular Graphic System,

582 version 1.4.1. (Schrödinger), and LIGPLOT [33] were used to generate illustrations and visualize

583 interactions.

4.3.1 PDB accession codes.

585 Coordinates and structure factors of have all been deposited in the Protein Data Bank with accession

586 numbers 6TMC (VIM-2_**1dh´**), 6TM9 (VIM-2_**1cc´**), 6TMB (VIM-2_**1di´**) and 6TMA (VIM-2_**1dj´)**.
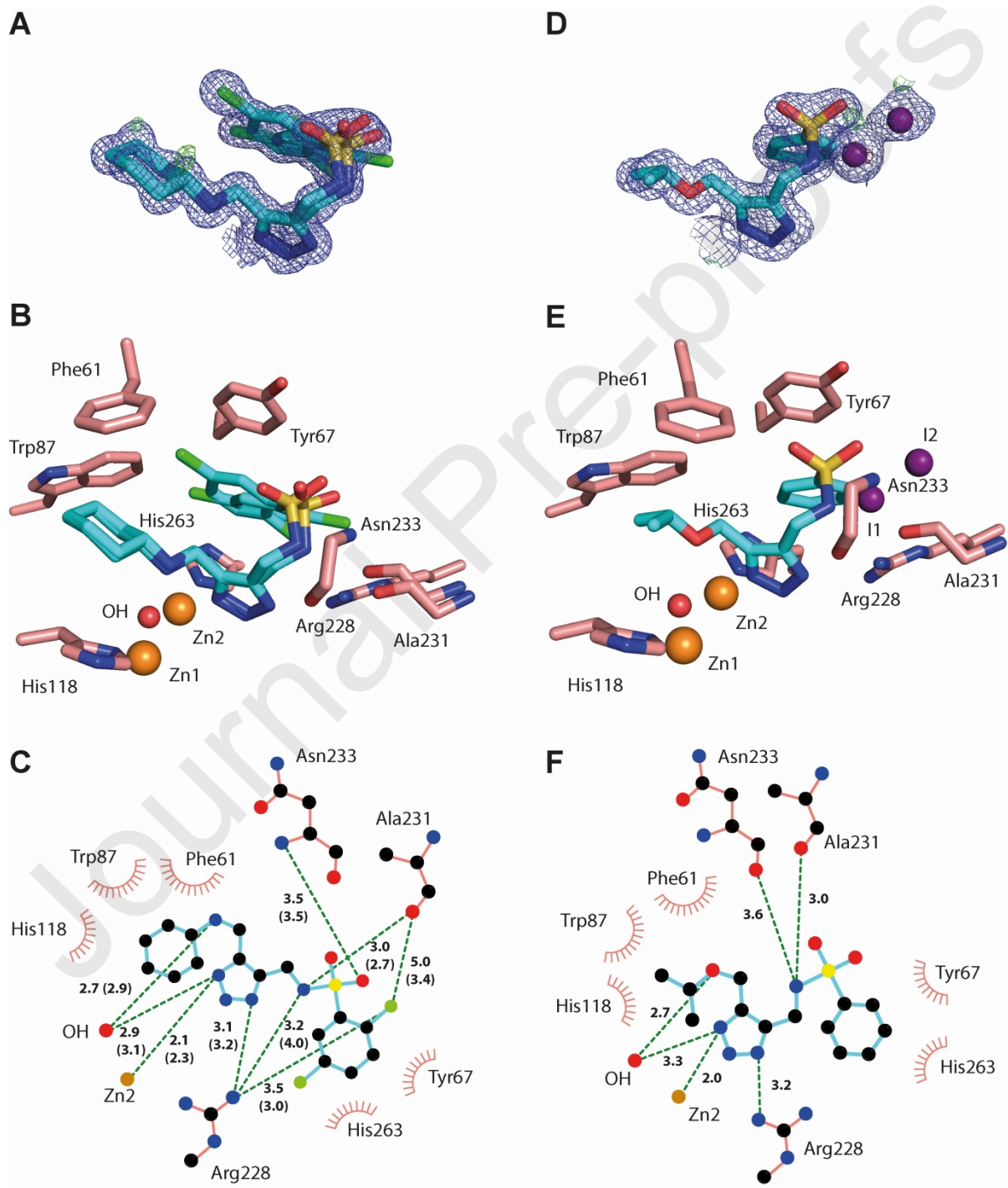
Acknowledgements

References

594 1. WHO, 2014, ISBN-978-992-974-156474-156478.

595 2. G. Patel and R. A. Bonomo, *Frontiers in microbiology*, 2013, **4**, 48.

596 3. T. R. Walsh, *Int. J. Antimicrob. Agents*, 2010, **36**, S8-S14.

597 4. J.-D. Docquier and S. Mangani, *Drug Resist. Updat.*, 2018, **36**, 13-29.

598 5. K. Bush and P. A. Bradford, *Nat. Rev. Microbiol.*, 2019, **17**, 295-306.

599 6. K. A. Toussaint and J. C. Gallagher, *Ann. Pharmacother.*, 2015, **49**, 86-98.

600 7. M. Everett, N. Sprynski, A. Coelho, J. Castandet, M. Bayet, J. Bougnon, C. Lozano, D. T.
601 Davies, S. Leiris, M. Zalacain, I. Morrissey, S. Magnet, K. Holden, P. Warn, F. De Luca,
602 J.-D. Docquier and M. Lemonnier, *Antimicrob Agents Chemother*, 2018, **62**, e00074-
603 00018.

604 8. A. M. King, S. A. Reid-Yu, W. Wang, D. T. King, G. De Pascale, N. C. Strynadka, T. R.
605 Walsh, B. K. Coombes and G. D. Wright, *Nature*, 2014, **510**, 503-506.

606 9. S. K. Yang, J. S. Kang, P. Oelschlaeger and K. W. Yang, *ACS Med. Chem. Lett.*, 2015, **6**,
607 455-460.

608 10. M. M. González, M. Kosmopoulou, M. F. Mojica, V. Castillo, P. Hinchliffe, I. Pettinati, J.
609 Brem, C. J. Schofield, G. Mahler, R. A. Bonomo, L. I. Llarrull, J. Spencer and A. J. Vila,
610 *ACS Infect. Dis.*, 2015, **1**, 544–554.

611 11. F. Spyrakis, G. Celenza, F. Marcoccia, M. Santucci, S. Cross, P. Bellio, L. Cendron, M.
612   Perilli and D. Tondi, *ACS Med. Chem. Lett.*, 2018, **9**, 45-50.
613 12. L. Sevaille, L. Gavara, C. Bebrone, F. De Luca, L. Nauton, M. Achard, P. Mercuri, S.
614   Tanfoni, L. Borgianni, C. Guyon, P. Lonjon, G. Turan-Zitouni, J. Dzieciolowski, K. Becker,
615   L. Benard, C. Condon, L. Maillard, J. Martinez, J. M. Frere, O. Dideberg, M. Galleni, J. D.
616   Docquier and J. F. Hernandez, *ChemMedChem*, 2017, **12**, 972-985.
617 13. T. Weide, S. A. Saldanha, D. Minond, T. P. Spicer, J. R. Fotsing, M. Spaargaren, J. M.
618   Frere, C. Bebrone, K. B. Sharpless, P. S. Hodder and V. V. Fokin, *ACS Med. Chem. Lett.*,
619   2010, **1**, 150-154.
620 14. D. Minond, S. A. Saldanha, P. Subramaniam, M. Spaargaren, T. Spicer, J. R. Fotsing, T.
621   Weide, V. V. Fokin, K. B. Sharpless, M. Galleni, C. Bebrone, P. Lassaux and P. Hodder,
622   *Bioorg. Med. Chem.*, 2009, **17**, 5027-5037.
623 15. S. Skagseth, S. Akhter, M. H. Paulsen, Z. Muhammad, S. Lauksund, Ø. Samuelsen, H.-K.
624   S. Leiros and A. Bayer, *Eur. J. Med. Chem.*, 2017, **135**, 159-173.
625 16. T. Christopeit, K.-W. Yang, S.-K. Yang and H.-K. S. Leiros, *Acta Crystallogr. F Struct. Biol.*
626   *Commun.*, 2016, **72**, 813-819.
627 17. T. Christopeit, T. J. Carlsen, R. Helland and H.-K. S. Leiros, *J. Med. Chem.*, 2015, **58**,
628   8671-8682.
629 18. H. Zhang and Q. Hao, *FASEB J.*, 2011, **25**, 2574-2582.
630 19. P. S. Borra, Ø. Samuelsen, J. Spencer, T. R. Walsh, M. S. Lorentzen and H.-K. S. Leiros,
631   *Antimicrob Agents Chemother*, 2013, **57**, 848-854.
632 20. J. C. Loren and K. B. Sharpless, *Synthesis*, 2005, **9**, 1514-1520.
633 21. K. Banert, *Chem. Ber.*, 1989, **122**, 911-918.
634 22. K. Banert, M. Hagedorn, C. Hemeltjen, A. Ihle, K. Weigand and H. Priebe, *Arkivoc*, 2016,
635   **2016**, 338-361.
636 23. K. Banert and M. Hagedorn, *Angewandte Chemie International Edition in English*, 1989,
637   **28**, 1675-1676.
638 24. J. R. Alexander, M. H. Packard, A. M. Hildebrandt, A. A. Ott and J. J. Topczewski, *The*
639   *Journal of Organic Chemistry*, 2020, **85**, 3174-3181.
640 25. T. Christopeit and H.-K. S. Leiros, *Bioorg. Med. Chem. Lett.*, 2016, **26**, 1973-1977.
641 26. Y. Yamaguchi, W. Jin, K. Matsunaga, S. Ikemizu, Y. Yamagata, J. Wachino, N. Shibata, Y.
642   Arakawa and H. Kurosaki, *J. Med. Chem.*, 2007, **50**, 6647-6653.
643 27. M. Aitha, A. R. Marts, A. Bergstrom, A. J. Moller, L. Moritz, L. Turner, J. C. Nix, R. A.
644   Bonomo, R. C. Page, D. L. Tierney and M. W. Crowder, *Biochemistry*, 2014, **53**, 7321-
645   7331.
646 28. I. Garcia-Saez, J. D. Docquier, G. M. Rossolini and O. Dideberg, *J. Mol. Biol.*, 2008, **375**,
647   604-611.
648 29. H.-K. S. Leiros, J. Timmins, R. B. Ravelli and S. M. McSweeney, *Acta Crystallogr. D Biol.*
649   *Crystallogr.*, 2006, **62**, 125-132.
650 30. R. B. Ravelli, H.-K. S. Leiros, B. Pan, M. Caffrey and S. McSweeney, *Structure*, 2003, **11**,
651   217-224.
652 31. H. K. Leiros, S. M. McSweeney and A. O. Smalas, *Acta Crystallogr. D Biol. Crystallogr.*,
653   2001, **57**, 488-497.
654 32. J. Chen, Y. F. Liu, T. Y. Cheng, X. Z. Lao, X. D. Gao, H. Zheng and Y. W. B., *Med. Chem.*
655   *Res.*, 2014, **23**, 300-309.
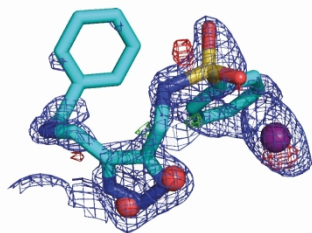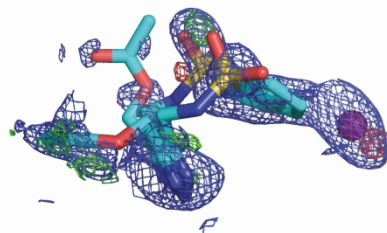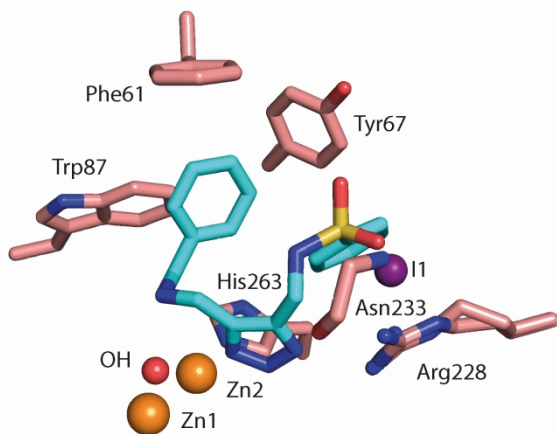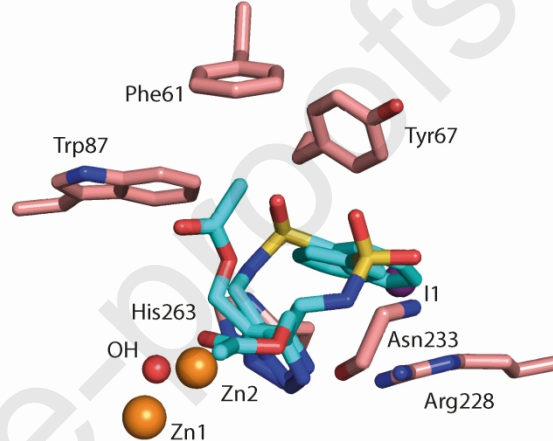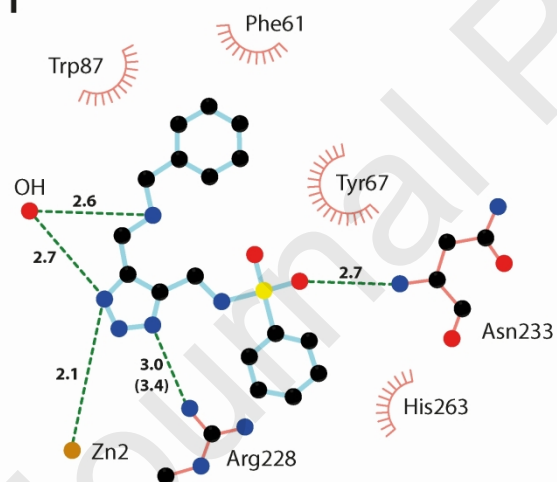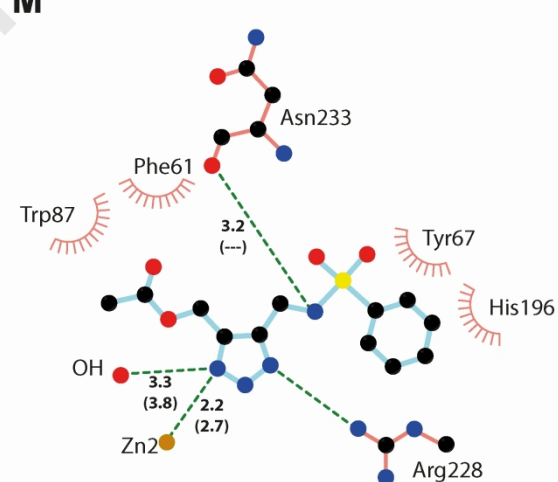656 33. A. C. Wallace, R. A. Laskowski and J. M. Thornton, *Protein Eng.*, 1995, **8**, 127-134.

657 34. M. Castanheira, M. A. Toleman, R. N. Jones, F. J. Schmidt and T. R. Walsh, *Antimicrob.*
658   *Agents Chemother.*, 2004, **48**, 4654-4661.
659 35. D. Yong, M. A. Toleman, C. G. Giske, H. S. Cho, K. Sundman, K. Lee and T. R. Walsh,
660   *Antimicrob. Agents Chemother.*, 2009, **53**, 5046-5054.
661 36. K. K. Kumarasamy, M. A. Toleman, T. R. Walsh, J. Bagaria, F. Butt, R. Balakrishnan, U.
662   Chaudhary, M. Doumith, C. G. Giske, S. Irfan, P. Krishnan, A. V. Kumar, S. Maharjan, S.
663   Mushtaq, T. Noorie, D. L. Paterson, A. Pearson, C. Perry, R. Pike, B. Rao, U. Ray, J. B.
664   Sarma, M. Sharma, E. Sheridan, M. A. Thirunarayan, J. Turton, S. Upadhyay, M. Warner,
665   W. Welfare, D. M. Livermore and N. Woodford, *Lancet Infect. Dis.*, 2010, **10**, 597-602.
666 37. H.-K. S. Leiros, K. S. Edvardsen, G. E. Bjerga and Ø. Samuelsen, *FEBS J.*, 2015, **282**, 1031-
667   1042.
668 38. Ø. Samuelsen, M. Castanheira, T. R. Walsh and J. Spencer, *Antimicrob. Agents*
669   *Chemother.*, 2008, **52**, 2905-2908.
670 39. G. Garau, C. Bebrone, C. Anne, M. Galleni, J. M. Frere and O. Dideberg, *J. Mol. Biol.*,
671   2005, **345**, 785-795.
672 40. E. A. Rogulin, T. A. Perevyazova, L. A. Zheleznaya and N. I. Matvienko, *Biochemistry-*
673   *Moscow+*, 2004, **69**, 1123-1127.
674 41. U. K. Laemmli, *Nature*, 1970, **227**, 680-685.
675 42. N. Laraki, N. Franceschini, G. M. Rossolini, P. Santucci, C. Meunier, E. de Pauw, G.
676   Amicosante, J. M. Frère and M. Galleni, *Antimicrob. Agents Chemother.*, 1999, **43**, 902-
677   906.
678 43. S. Siemann, D. P. Evanoff, L. Marrone, A. J. Clarke, T. Viswanatha and G. I. Dmitrienko,
679   *Antimicrob Agents Chemother*, 2002, **46**, 2450-2457.
680 44. Q. Sun, A. Law, M. W. Crowder and H. M. Geysen, *Bioorg. Med. Chem. Lett.*, 2006, **16**,
681   5169-5175.
682 45. T. Christopeit, A. Albert and H.-K. S. Leiros, *Bioorg. Med. Chem.*, 2016, **24**, 2947-2953.
683 46. W. Kabsch, *Acta Crystallogr. D Biol. Crystallogr.*, 2010, **66**, 125-132.
684 47. P. R. Evans, *Acta Crystallogr D Biol Crystallogr*, 2011, **67**, 282-292.
685 48. P. Evans, *Acta Crystallogr. D Biol. Crystallogr.*, 2006, **62**, 72-82.
686 49. A. J. McCoy, R. W. Grosse-Kunstleve, P. D. Adams, M. D. Winn, L. C. Storoni and R. J.
687   Read, *J. Appl. Crystallogr.*, 2007, **40**, 658-674.
688 50. P. D. Adams, P. V. Afonine, G. Bunkoczi, V. B. Chen, I. W. Davis, N. Echols, J. J. Headd,
689   L. W. Hung, G. J. Kapral, R. W. Grosse-Kunstleve, A. J. McCoy, N. W. Moriarty, R.
690   Oeffner, R. J. Read, D. C. Richardson, J. S. Richardson, T. C. Terwilliger and P. H. Zwart,
691   *Acta Crystallogr. D Biol. Crystallogr.*, 2010, **D66**, 213-221.
692 51. P. Emsley, B. Lohkamp, W. G. Scott and K. Cowtan, *Acta Crystallogr. D Biol. Crystallogr.*,
693   2010, **66**, 486-501.
694
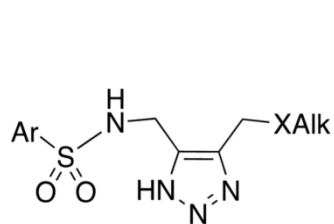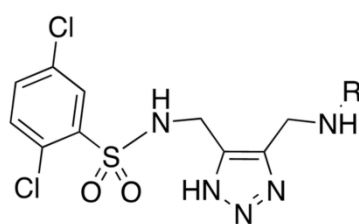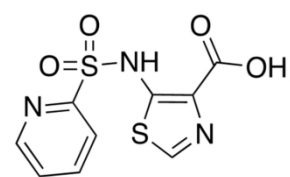
G

K

H

Phe61
Tyr67
Trp87
His263
I1
Asn233
Arg228
OH
Zn2
Zn1

L

Phe61
Trp87
Tyr67
His263
I1
Asn233
OH
Zn2
Arg228
Zn1

I

Phe61
Trp87
OH 2.6
2.7
Tyr67
2.7
Asn233
2.1
3.0
(3.4)
His263
Zn2
Arg228

M

Asn233
Phe61
Trp87
3.2
(---)
Tyr67
His196
OH 3.3
(3.8)
2.2
(2.7)
Zn2
Arg228

697

A: Synthetic pathway[13]

R^1 : a = (phenyl)   b = (p-tolyl)   c = (2,5-dichlorophenyl)   d = (p-iodophenyl)

R^2 : a´ = $-NH_2$ b´ = $-O-$tBu   c´ = $-NH-$cyclohexyl   d´ = $-NH-$adamantyl   e´ = $-NH-$trityl   f´ = $-S-CH_2-$(p-methoxyphenyl)   g´ = $-O-$

h´ = $-O-$iPr   i´ = $-NH-$benzyl   j´ = $-O-$acetyl

B: Mechanistic view of the Banert cascade[21, 23, 24]

698

1dj'*
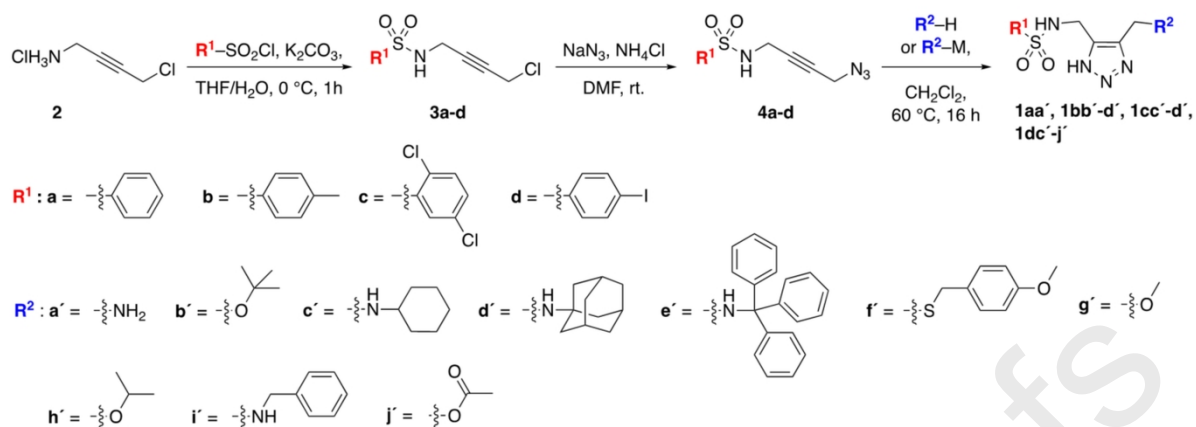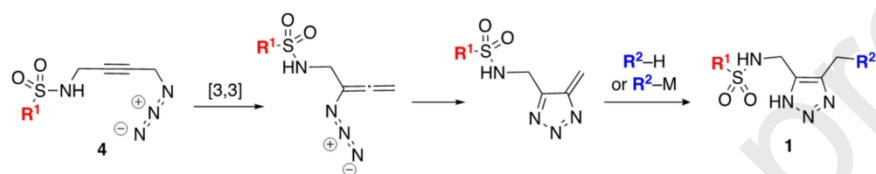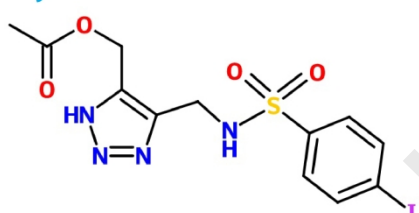
IC$_{50}$ (**1dj'***)

VIM-2	23 μM
GIM-1	48 μM
NDM-1	231 μM
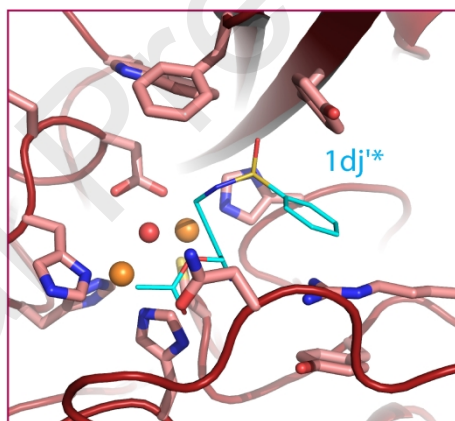
MIC for **1dj'*** towards
P. aeruginosa with VIM-2

1 mg/mL

699